People's Demoratic Republic of Algeria

Ministry of Higher Education and Scientific Research

Mohamed Boudiaf University – M'Sila

Faculty Of Technology
Department Of Electrical
Engineering No : Elm-1

FIELD : ELECTROMECHANICS

DOMAIN: ELECTROMECHANICS

Thesis submitted in partial

fulfillment of the requirements for the degree

of Academic Master's

By: BOUACHERINE Belkacem

Subject

Optimization of magnets in a buried magnet synchronous motor

Defended before the jury composed of :

Dr.BELHAOUCHET Khaled	Mohamed Boudiaf University of M'Sila	President
Dr. ZORIG Assam	Mohamed Boudiaf University of M'Sila	Rapporteur
Dr.HAMOUDA Noureddine	Mohamed Boudiaf University of M'Sila	Supervisor
Dr.GHADBAN Ismail	Mohamed Boudiaf University of M'Sila	Examiner

Academic Year: 2024 / 2025


بسم الله الرحمن الرحيم

Dedication

To my beloved parents,

To my mother, the source of my prayers

To my father Said, a source of inspiration and strength,

To my entire family for their unconditional support,

And to all my friends, for their support and companionship

throughout this academic journey.

Acknowledgments

First and foremost, I thank **ALLAH** Almighty for granting me the strength and determination to complete this work.

I would like to express my sincere gratitude to my thesis supervisor, Mr. **ZORIG Assam**, for his patience, availability, and especially for his valuable guidance, which greatly contributed to shaping my ideas and directing my progress.

Finally, I offer my most respectful thanks to all the jury members who accepted to evaluate my work and enrich the defense with their constructive feedback.

ملخص

هذا العمل يتناول نمذجة وتحسين أداء آلة تزامنية ذات مغناطيسات دائمة مدفونة Interior Permanent Magnet Synchronous Motor(IPMSM)، وهي عنصر أساسي في التطبيقات الحديثة للهندسة الكهربائية مثل المركبات الكهربائية وأنظمة القيادة الصناعية. باستخدام برنامجي Flux 2D وHyperStudy، تم إجراء محاكاة وتحسين للآلة بهدف تقليل تموجات العزم وتقليل الفواقد مع الحفاظ على قيمة العزم المتوسط ثابتة. يُظهر النموذج المحسَّن كفاءة أفضل، واستقرارًا أكبر في السلوك الكهرومغناطيسي، وتحويلًا أكثر فاعلية للطاقة. تُبرز هذه الدراسة أهمية أدوات المحاكاة والتحسين في تحسين أداء وموثوقية الآلات الكهربائية، وهو مجال رئيسي في الهندسة الكهربائية. علاوة على ذلك، كان أحد الأهداف الرئيسية هو تقليل مساحة المغناطيس، وقد تحقق هذا الهدف بالفعل من خلال عملية التحسين.

Résumé

Ce travail porte sur la modélisation et l’optimisation d’une machine synchrone à aimants permanents enfouis (Interior Permanent Magnet Synchronous Motor IPMSM), un composant essentiel dans les applications modernes du génie électrique telles que les véhicules électriques et les entraînements industriels. À l’aide des logiciels Flux 2D et HyperStudy, la machine a été simulée et optimisée afin de réduire les ondulations de couple et les pertes tout en maintenant le couple moyen constant. Le modèle optimisé montre un meilleur rendement, un comportement électromagnétique plus stable et une conversion d’énergie plus efficace. Cette étude met en évidence l’importance des outils de simulation et d’optimisation pour améliorer les performances et la fiabilité des machines électriques, un domaine clé du génie électrique.De plus, l’un des objectifs principaux était de réduire la surface des aimants, et cet objectif a été atteint avec succès grâce au processus d’optimisation.

Abstract

This work focuses on the modeling and optimization of an Interior Permanent Magnet Synchronous Motor (IPMSM), a critical component in modern electrical engineering applications such as electric vehicles and industrial drives. Using Flux 2D and HyperStudy, the motor was simulated and optimized to reduce torque ripple and losses while maintaining the average torque. The optimized design demonstrates improved efficiency, smoother electromagnetic behavior, and better energy conversion. This study highlights the essential role of simulation and optimization tools in advancing the performance and reliability of electrical machines—one of the key areas of electrical engineering. Moreover, one of the main objectives was to reduce the magnet area, and this goal was successfully achieved through the optimization process.

Table of Contents

List of Figures

Chapter 1

Chapter 2

Chapter 3

List of Tables

Chapter 1

Chapter 2

Chapter 3

List of Symbols and Abbreviations

Abbreviation / Symbol	Meaning	Unit
PM motor	Permanent Magnet Motor	
PMSM	Permanent Magnet Synchronous Motor	
IPMSM	Interior Permanent Magnet Synchronous Motor	
SPMSM	Surface Permanent Magnet Synchronous Motor	
WRSM	Wound Rotor Synchronous Machine	
DESM	Doubly Excited Synchronous Machine	
ACM / MAS	Asynchronous Machine	
NdFeB	Neodymium-Iron-Boron (Magnetic Material)	
SmCo	Samarium-Cobalt (Magnetic Material)	
FEM	Finite Element Method	
FOC	Field-Oriented Control	
Ns	Synchronous Speed	RPM
fs	Frequency of AC Supply	Hz
P	Number of Poles	
p	Number of Pole Pairs (= P/2)	
C	Torque	N·m
m	Magnetic Moment	A·m²
B	Magnetic Field / Flux Density	T
μr	Relative Permeability	
ρ (rho)	Electrical Resistivity	Ω·m
J	Current Density	A/m²
E	Electric Field	V/m
H	Magnetic Field Strength	A/m
Br	Remanent Flux Density	T
DOE	Design of Experiments	
GRSM	Global Response Surface Method	
SQP	Sequential Quadratic Programming	
AI	Artificial Intelligence	
BEMF	Back Electromotive Force	V
rpm	Rotations Per Minute	
I1, I2, I3	Phase Currents	A
AngSpeed(ROTOR)	Angular Speed of Rotor	rad/s
EMF	Electromotive Force	V
AFPM	Axial Flux Permanent Magnet	
RFPM	Radial Flux Permanent Magnet	
SynRM	Synchronous Reluctance Motor	
Curie Temperature	Critical temperature above which magnetism vanishes	°C

General introduction

In response to the rapid transformation of the energy and transportation sectors fueled by the global pursuit of electrification, environmental sustainability, and energy efficiency electric machines have become a cornerstone of modern engineering applications. Among the various technologies, Interior Permanent Magnet Synchronous Motors (IPMSMs) have gained prominence due to their superior performance, including high torque density, excellent efficiency, and strong field weakening capability. These characteristics make IPMSMs ideal for high-speed applications such as electric vehicles, spindle drives, and machine tools.

Compared to Surface Permanent Magnet Synchronous Motors (SPMSMs), IPMSMs exhibit enhanced mechanical integrity due to their rotor structure, which embeds the magnets securely within the core, eliminating the need for additional reinforcement at high rotational speeds. This not only improves durability but also reduces the amount of magnetic material required for achieving the same torque density.

Furthermore, the ability of IPMSMs to maintain constant power over a wide speed range makes them highly attractive for traction applications in electric mobility. Previous research has extensively analyzed the influence of various design parameters including d-axis inductance, permanent magnet flux linkage, number of pole pairs, and maximum current on the torque-speed characteristics of these machines . In the context of e-mobility, ensuring smooth motor operation is essential, which has led researchers to focus on reducing cogging torque through geometric optimization of both stator and rotor components[1].

To achieve further improvements, modern motor development integrates advanced simulation tools such as those based on the Finite Element Method (FEM), like Altair Flux, which provide accurate insights into magnetic flux behavior, torque production, and power losses. However, simulation alone is not sufficient to reach optimal design configurations. This is where multi-objective optimization platforms like Altair HyperStudy come into play

enabling engineers to evaluate complex trade-offs across multiple performance criteria and explore a wide range of design possibilities[2].

This research focuses on the performance analysis and design enhancement of an IPMSM. The study evaluates electromagnetic torque, magnetic flux distribution, and loss characteristics using FEM-based simulation. In addition, an optimization strategy targeting the geometry of embedded magnets is implemented to enhance torque smoothness, overall efficiency, and material usage. The outcomes of pre- and post-optimization analyses are compared to validate the effectiveness of the proposed improvements[3].

Chapter 1 General Concepts of Permanent Magnet Synchronous Machines

1 Introduction

Permanent magnet synchronous motors (PM motors) are among the most prominent solutions in modern systems that require high efficiency and strong torque. These motors rely on different permanent magnets, such as Neodymium-Iron-Boron (NdFeB) and Samarium-Cobalt (SmCo), which contribute to improved performance by providing high levels of torque and efficiency, as well as their ability to operate across a wide range of speeds[4]. The motor's efficiency is greatly influenced by the type of magnet and the surrounding temperature. When exposed to high temperatures, magnets may lose their magnetism, reducing their effectiveness and, in turn, affecting motor performance. Permanent magnet synchronous motors find applications in various fields such as industrial machinery, transportation systems, robotics, and renewable energy systems, helping to improve performance and reduce energy consumption[5].

2 Overview of Machines

2.1 Asynchronous Motors (ACM)

Asynchronous motors (ACM) are electrical machines that operate at high rotation speeds and are widely used in energy-saving electric drive systems due to their capability of frequency control[6].

2.2 Synchronous Machine

Although more complex to control, more expensive, and potentially less robust, the synchronous motor has become the preferred choice in electric and hybrid vehicles. The synchronous machine provides the highest efficiency in both generator and motor modes. Like the asynchronous motor, the synchronous motor consists of a stator and a rotor separated by an air gap. The only difference lies in the rotor design.

2.2.1 Three Types of Synchronous Machines

Three families of synchronous machines are in competition:

2.2.1.1 Wound Rotor Synchronous Machine (WRSM)

These machines use windings to create the rotor field, which can be electronically adjusted, allowing easy control at high speeds (flux weakening). However, WRSMs require electrical contact with the rotor through a brush-collector system.

A raw material with rising costs.

2.2.1.2 Doubly Excited Synchronous Machine (DESM)

These machines aim to combine the benefits of PMSMs (high energy efficiency) with those of WRSMs (ease of variable-speed operation). The excitation flux in these machines is the sum of a flux generated by permanent magnets and a flux created by windings[7].

2.2.1.3 Permanent Magnet Synchronous Machine (PMSM)

A Permanent Magnet Synchronous Motor (PMSM) consists of conventional three-phase windings in the stator and permanent magnets in the rotor. In traditional synchronous motors, field windings are used to generate the magnetic field, but in PMSM, these windings are replaced with permanent magnets, which improves efficiency and eliminates the need for an additional excitation power source. PMSM has seen significant development due to the discovery of new magnetic materials and rare earth elements, enhancing its performance and efficiency. These motors offer numerous advantages, making them ideal for modern motion control systems. Additionally, the availability of high magnetic flux density materials has helped optimize their design, making them more energy-efficient.

In synchronous motors, the rotor rotates at the same speed as the rotating magnetic field in the stator. This speed is known as the synchronous speed, which depends on the electrical frequency (fs) and the number of pole pairs (p) in the stator. It can be calculated using the following equation:

$$Ns = {}^{120fs}/_{P} \quad (1)$$

Where:

Ns = Synchronous speed (Revolutions Per Minute - RPM).

fs = Frequency of the AC supply (Hertz - Hz).

P = Number of poles in the motor.

p = Number of pole pairs (P/2).

When a PMSM is supplied with three-phase AC power, a rotating magnetic field is generated in the stator, which interacts with the permanent magnets embedded in the rotor. This interaction produces torque, ensuring that the rotor stays synchronized with the stator's magnetic field. The performance and torque generation of PMSM depend on the magnetic material properties, the number of poles, and the stator and rotor design. Torque and speed control are enhanced using Field-Oriented Control (FOC) techniques, enabling precise and efficient motor operation.

Thanks to its high efficiency and excellent torque density, PMSM is widely used in various applications, including electric vehicles, precision motion control systems such as robotics, industrial pumps and fans, and medical equipment. PMSM is considered one of the most efficient electric motors, as it relies on permanent magnets instead of electrical excitation, eliminating the need for an additional power source for the magnetic field. This design enhances performance and reduces energy consumption, making it ideal for applications requiring high precision and efficiency Table 1 [8, 9].

Table 1: Comparative Table of Different Presented Machines[7]

Machine Type	Advantages	Disadvantages
Asynchronous Machine (MAS)	Well-established manufacturing, high power-to-mass ratio, robust motor, easy overspeed operation, long lifespan.	Low efficiency, rotor Joule losses, low starting torque, expensive electronics, complex control.
Wound Rotor Synchronous Machine (MSRB)	Variable flux for easy control, no magnets required, wide speed range.	Bulkier and heavier than MSAP, requires additional electronics (chopper), fragile slip-ring system.
Permanent Magnet Synchronous Machine (MSAP)	Common technology, high power-to-mass ratio, no rotor heating, very high efficiency, easy cooling.	Torque ripple, high cost of magnets, expensive technology, overspeed limitations, difficult field weakening.

Double Excitation Synchronous Machine (MSDE)	Good efficiency, relatively high power-to-mass ratio, wide speed range (easy field weakening).	Fragile slip rings, requires additional electronics (chopper).

Although current designs face challenges such as torque ripple, high magnet costs, expensive technology, overspeed limitations, and difficulties in field weakening, these issues also offer clear opportunities for improvement. Reducing torque ripple can lead to smoother, more efficient operation, while exploring cost-effective magnet alternatives may help lower manufacturing expenses. Additionally, optimizing the underlying technology could result in more affordable and competitive motor solutions. Enhancing overspeed capabilities and developing more efficient field weakening strategies would further expand the operational range and flexibility of these machines, ultimately elevating their overall performance.

2.3 Permanent magnets:

Permanent magnets are unique in their ability to deliver magnetic flux into the air gap of a magnetic circuit without any continuous energy expenditure . The flux density can be uniform or non-uniform, and it may be either steady or time varying. Moreover, magnet applications can be categorized based on either their influence on the magnet or the specific physical effect they exploit. Table 2 provides a summary of these applications. Although the list is extensive, the full potential of permanent magnets is only just beginning to be appreciated and utilized. Their versatility and cost-effectiveness have paved the way for numerous new applications, in addition to replacing electromagnets in many areas.

In the following, we briefly discuss the various physical effects mentioned in the table. For example, a steady uniform field can be employed to generate torque or to align existing magnetic moments, as expressed by the relationship:$C=m\cdot B$

where C is the torque, mm is the magnetic moment, and B is the magnetic field[10].

Table 2: Summary of Permanent Magnet Applications[10]

Field	Magnetic Effect	Type	Examples
Uniform	Zeeman splitting	Static	Magnetic resonance imaging
	Torque		Alignment of magnetic powder
	Hall effect, magnetoresistance		Sensors, read-heads
	Force on conductor	Dynamic	Motors, actuators, loudspeakers
	Induced emf		Generators, microphones
Non Uniform	Force on charged particles	Static	Beam control, radiation sources (microwave, UV, X-ray)
	Force on magnet	Dynamic	Bearings, couplings, Maglev
	Force on paramagnet		Mineral separation
	Force on iron		Switchable clamps, holding magnets
Time Varying	Varying field		Magnetometers
	Eddy currents		Metal separation, brakes

3 Classification of Permanent Magnet Motors

Permanent magnet motors are generally categorized into two main types: brushless DC (BLDC) motors and permanent magnet synchronous motors (PMSMs) [11]. The classification of permanent magnet synchronous machines is based on the arrangement of magnets on the rotor. Their configurations include radial flux (RFPM) and axial flux (AFPM) machines. These machines can operate with either sinusoidal currents in the case of PMSMs or square-wave currents in the case of BDCMs. A schematic representation of the two types of permanent magnet machines, radial flux and axial flux, is shown in Figure 1 [12].

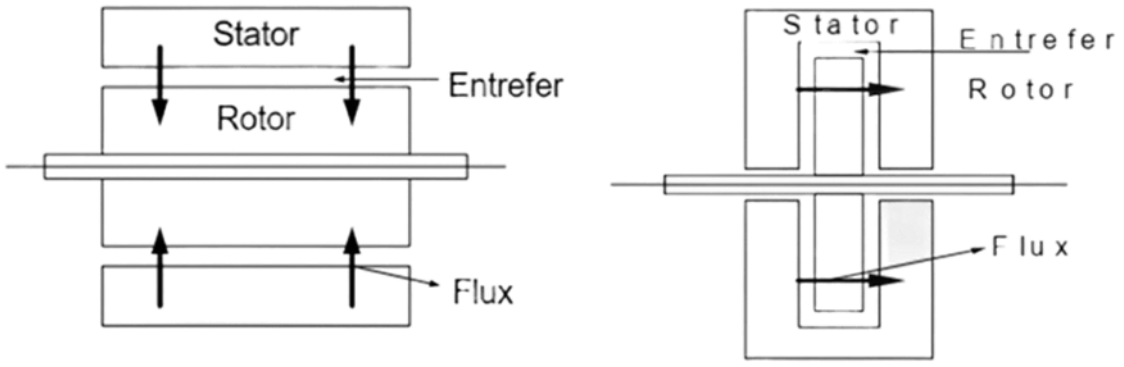

(a) (b)

Figure 1: (a) Radial Flux Direction (RFPM) , (b) Axial Flux Direction (AFPM) [13]

The characteristics of PMSMs strongly depend on rotor construction. PMSM rotor designs can be categorized into two main types: rotors with surface-mounted magnets and rotors with buried (Interior) magnets[14] Figure2[15] .

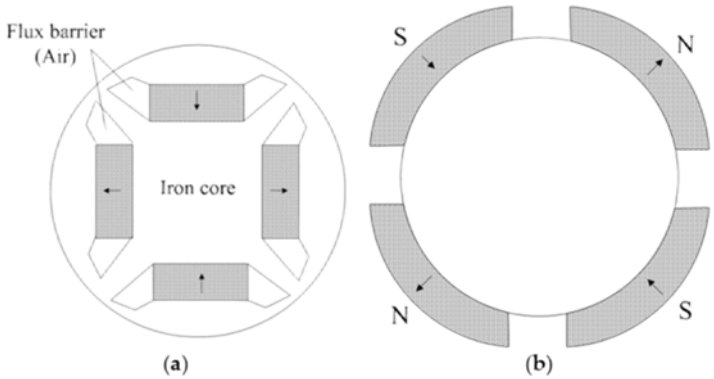

Figure 2: Permanent magnet synchronous motors (PMSM) rotor structures

(a) Embedded (Interior)type;(b) Surfaced-mounted type

3.1 Surface-Mounted Magnets

Surface-mounted magnets (a) are the most common configuration, where magnets are glued to the rotor. This design is relatively simple and cost-effective. However, it has some drawbacks, as the magnets remain exposed and vulnerable. First, they are significantly affected by armature reaction fields, which can lead to partial or complete demagnetization. Additionally, they are difficult to flux-weak. Second, in an internal rotor configuration, the magnets experience strong centrifugal forces, which may cause them to detach from the rotor.

To address these issues, magnet retention can be reinforced using a banding system. This approach provides benefits similar to embedded magnet designs, offering protection against corrosion, mechanical impacts, and dust. The bands can be made from non-magnetic materials such as fiberglass, carbon fiber, or Inconel, or from magnetic materials like copper, aluminum, or steel. Magnetic bands help shield permanent magnets from demagnetizing fields, provide asynchronous starting torque, or act as dampers. In this case, eddy current losses primarily occur in the band rather than in the magnet itself.

The main drawback of this method is the additional cost. It is also worth noting that, in some special cases, magnetization is not radial but tangential, which results in a more sinusoidal open-circuit electromotive force (EMF)[16].

Surface-mounted Permanent Magnet Synchronous Motors (PMSMs) with radial flux are typically used in low-speed applications. They offer the advantage of higher power density compared to other PMSM types.

On the other hand, Interior PMSMs (IPMSMs) are preferred for high-speed applications due to their robust rotor structure and ability to utilize reluctance torque effectively[17].

3.2 Buried (Interior) magnets

Interior (Buried) Permanent Magnet Synchronous Motor (IPMSM) machines (d) use rectangular magnets and flux barriers to manage leakage, increasing air-gap flux density[16]. The method of mounting permanent magnets on the rotor plays a crucial role in the variation of direct-axis (d-axis) and quadrature-axis (q-axis) inductance values[17]. (IPMSM) simplify the magnet manufacturing process. Unlike surface-mounted magnet machines, which typically have tile-shaped magnets with radial magnetization, buried magnet machines use rectangular magnets with parallel magnetization.

To prevent magnetic short circuits, flux barriers must be incorporated into the design. Compared to surface-mounted magnet machines, the flux leakage in these barriers is more significant than the leakage between magnets. This results in a reduction of the air-gap flux.

This design increases the air-gap flux density or allows the use of magnets with lower remanence. Such configurations are particularly well-suited for ferrite magnets. It is important to note that, in these machines, the magnetic poles form within the ferromagnetic regions[16].

There are multiple ways to construct a surface-mounted or embedded permanent magnet motor, each offering unique performance characteristics. Figure 3 illustrates the various configurations of these motor types.

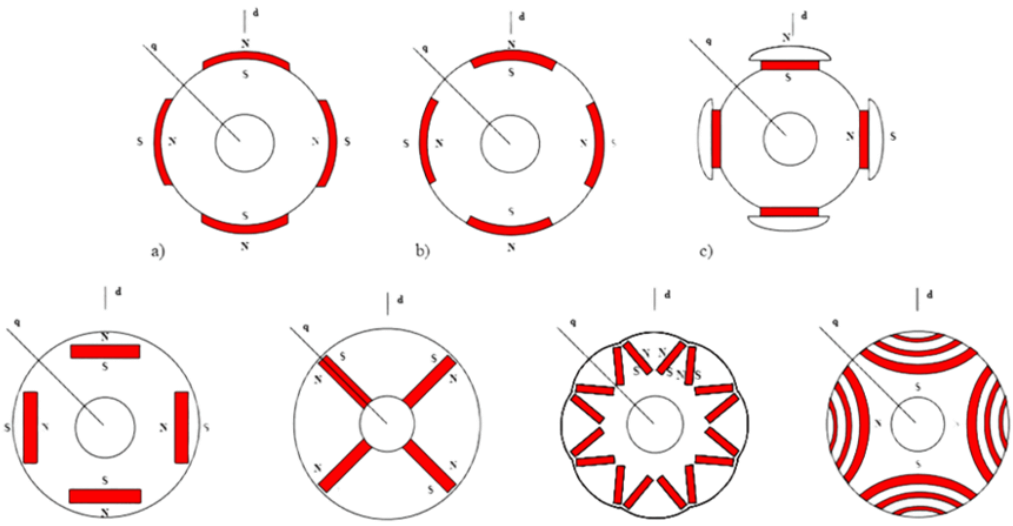

Figure 3: Location of the permanent magnets [18]

3.3 Classification of synchronous machines by torque

Figure 4 illustrates the ratio of magnet torque to reluctance torque in various synchronous machines. These machines can be categorized into three types based on their torque production principles.

Surface Permanent Magnet Synchronous Machine (SPMSM): In this type, arc-shaped permanent magnets are mounted on the rotor's surface, as shown in Figure 4 (a). It is a pure permanent magnet (PM) machine, generating only magnet torque.

Synchronous Reluctance Machine (SynRM): This is a pure reluctance machine that does not use permanent magnets, as depicted in Figure 4(f).

Interior Permanent Magnet Synchronous Machine (IPMSM): This machine features embedded permanent magnets inside the rotor core, as illustrated in Figures 4 (c–e). Due to its magnetic saliency, it is a hybrid PM/reluctance machine. The IPMSM can further be divided into:

Reluctance torque-assisted PMSM (Region II)

Permanent magnet torque-assisted SynRM (Region III)

3.4 Compared to SPMSM, IPMSM has several advantages

Reduced Eddy Current Losses: Unlike SPMSM, which typically requires a stainless-steel-can, IPMSM has a laminated rotor surface, significantly reducing eddy current losses.

Lower Magnet Cost: IPMSM uses square-shaped magnets instead of arc-shaped ones, leading to cost savings.

Utilization of Reluctance Torque: With Lq>Ld , reluctance torque is effectively harnessed alongside magnet torque.

Efficient Flux-Weakening Control: This enables high-speed operation and a wide constant-power range.

Enhanced Design Flexibility: IPMSM offers greater freedom in optimizing mechanical structure and torque-speed characteristics[19].

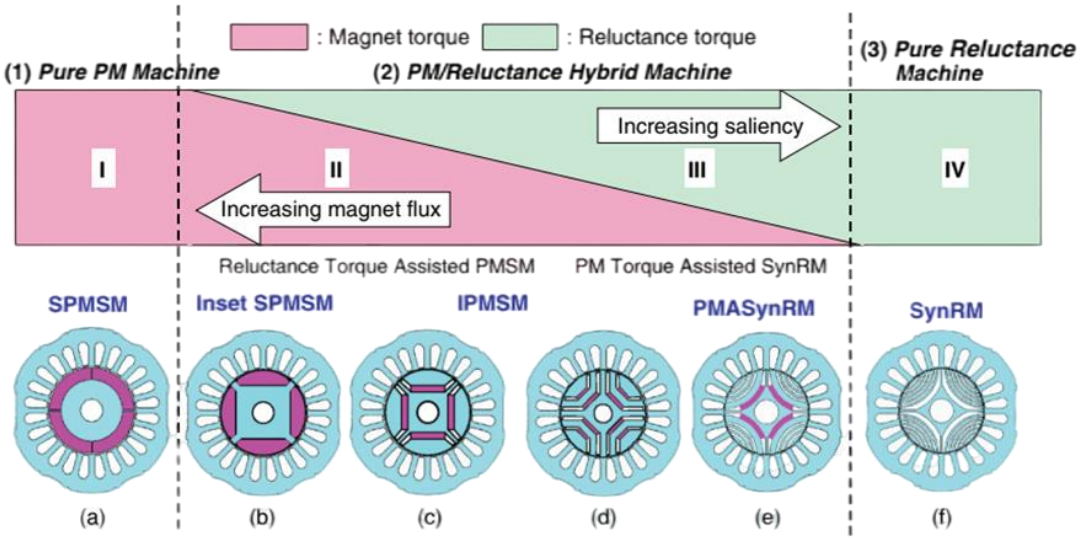

Figure 4: Classification of synchronous machines by torque generating mechanism[19]

4 Temperature Effects on Permanent Magnets

4.1 History and Applications of Permanent Magnets

Permanent magnets have been known since 600 B.C., with the Greek philosopher Thales of Miletus identifying loadstone (magnetite). The first artificial magnets were iron needles magnetized by loadstone. In the 12th century, magnets were used in compasses. Over time, significant advancements were made, including the development of electromagnets in 1825 and the discovery of alloys like Heusler, Alnico, and modern ferrites[20].

Today, most magnets are used in motors and actuators, which can operate at temperatures over 100°C. Research continues to develop materials for use at up to 400°C. However, as the Curie temperature is approached, both magnetization and coercivity decrease, limiting performance in high-temperature environments[10].

4.2 Permanent Magnets

Magnetic materials are classified based on the width of their hysteresis loop Figure 5 and are divided into two main categories. The first category consists of hard magnetic materials (with a wide loop), commonly known as "permanent magnets," as their magnetization remains unchanged under an external magnetic field. The second category includes soft magnetic materials, which exhibit magnetic properties only in the presence of an external excitation.

For rotor excitation, permanent magnets have replaced rotor windings for over two decades. Although they were known since ancient Greek times, significant advancements in permanent magnets only began in the 1930s. Today, there are four main families of permanent magnets: Alnico (or Ticonal), hard ferrites, Samarium-Cobalt, and Neodymium-Iron-Boron.

During the 1930s, Alnico magnets were the first to be industrialized. Composed of aluminum, nickel, and cobalt, they are now rarely used due to the high cost of cobalt and their relatively modest magnetic properties. However, niche applications such as measuring instruments and high-temperature environments still utilize these magnets for their excellent thermal stability[12, 13].

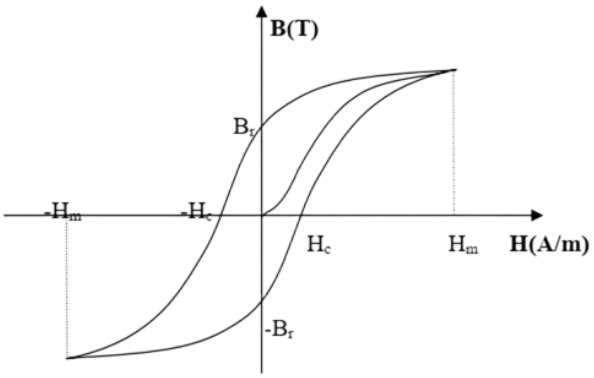

Figure 5 :Hysteresis cycle [12]

4.3 General Characteristics of Permanent Magnets

The operating state of a permanent magnet is located in the second quadrant of its hysteresis loop (see Figure 6).

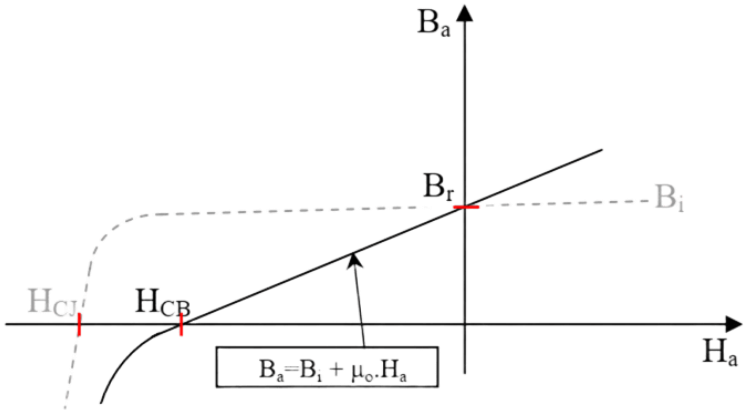

Figure 6 :Hysteresis loop

Permanent magnets are characterized by several key parameters that are crucial for industrial applications :

Residual Induction (Br): Indicates the potential power of the magnet and determines the necessary cross-section for maintaining the useful air-gap flux.

Coercive Field (HCB): Represents the magnetizing field required to cancel the residual induction. The higher its value, the more stable the magnet.

Intrinsic Coercive Field (HCJ): The field that completely cancels the intrinsic magnetization of the material, leading to total and irreversible demagnetization.

Maximum Energy Product ((B.H)max): Represents the energy value of the magnet per unit volume[12].

Rare-earth materials have enhanced the energy density of magnets. Samarium-Cobalt (SmCo) and Neodymium-Iron-Boron (NdFeB) magnets are characterized by high remanent induction, strong coercive field, and an almost linear B(H) characteristic in the second quadrant(see Figure 7)[16].

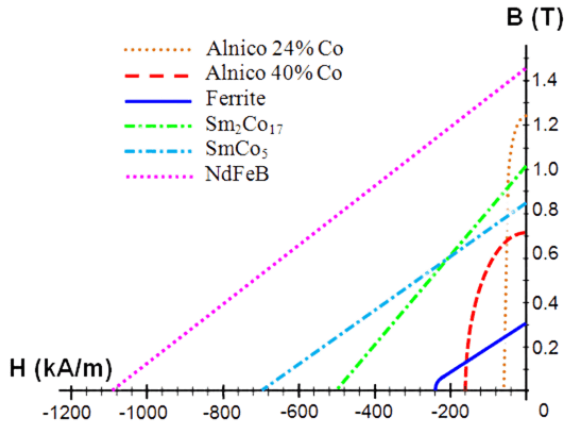

Figure 7: B-H characteristics of some materials

The choice of a magnet depends on the desired characteristics and its highly variable cost. Table 3 below provides some magnetic properties of different types of magnets.

Table 3: Examples of Magnetic Properties of Magnets[12]

Magnet Type	Energy Density (BH) max (kJ/m^3)	Remanent Induction Br (T) at 25°C	Coercive Field -Hc (kA/m)	Max Temperature Tmax (°C)	Price (€ / Kg)
NdFeB	200-380	1.2-1.5	900-2000	140-220	80-150
SmCo5	140-200	1	2000	280	220
Sm_2Co_{17}	180-240	1.05	2000	350-550	300
Alnico	50-85	1.1-1.3	130	550	45
Strontium Ferrite	27-35	0.3-0.4	250	250	6
Barium Ferrite	8-30	0.2-0.4	170	100-240	4.5

5 Stator Winding Design

The asynchronous motor consists of two main parts: the stator, which is the stationary component containing three windings that can be connected in either a star (Y) or delta (Δ) configuration based on the supply network, and the rotor, which is the rotating part. The rotor can either have a winding (typically three-phase, like the stator), accessible via three rings and brushes, or a squirrel-cage rotor made of aluminum bars, which is non-accessible. In both cases, the rotor circuit is short-circuited using rings or a rheostat. This configuration is critical for efficient energy transfer and motor performance Figure 8 [7].

To maximize efficiency, the motor employs a distributed winding technique, the most commonly used in industry. This method ensures a nearly sinusoidal distribution of the winding and magnetic field in the air gap, which significantly improves the stator's ability to recover rotor flux and minimizes magnetic losses. This design enables the motor to develop higher torque. However, it comes with a drawback: the substantial amount of copper needed for its implementation due to the coil heads, which adds to the overall cost and volume[16].

Figure 8: Distributed winding

6 Applications of Permanent Magnet Synchronous Machines

Interior Permanent Magnet (IPM) Synchronous Motor: High Efficiency, High Power Factor, and High Torque Density[21]:

Permanent magnet (PM) synchronous motors, particularly interior permanent magnet (IPM) synchronous motors, are widely used due to their high efficiency, high power factor, and high torque density. They are commonly applied in various industrial and transportation sectors, including:

Industrial Applications: Used in pumps, fans, compressors, servo drives, automation processes, and robotic systems.

Transportation: Implemented in electric and hybrid vehicles, elevators, escalators, and light rail systems.

Aerospace and Defense: Applied in aircraft control systems, electric ships, submarines, and military equipment.

Renewable Energy: Used in wind turbines and other energy conversion systems.

IPM motors offer superior performance in applications requiring precise control, high efficiency, and compact design[20].

7 Conclusion

Permanent magnet synchronous motors (PMSMs) play a crucial role in modern technology, acting as essential components for achieving high efficiency, reduced energy consumption, and reliable performance across a wide range of applications. Through the optimal use of permanent magnets, these motors are widely adopted in industrial, commercial, and transportation sectors. Ongoing improvements in magnetic material properties, manufacturing techniques, and the understanding of temperature effects continue to enhance their performance. Nevertheless, there remains significant scope for further research and development to optimize motor functionality for future use in diverse and demanding environments.

Chapter 2 Electromagnetic Equations and Motor Design Simulation

1 Introduction

The analysis and simulation of electromagnetic behavior in electrical machines, particularly Permanent Magnet Synchronous Motors (PMSMs), require a robust understanding of the governing physical laws and their accurate numerical implementation. This chapter, titled Electromagnetic Equations and Motor Design Simulation, aims to present a comprehensive framework that combines the fundamental theory of electromagnetism with practical simulation methodologies to study and improve motor performance[22].

We begin by revisiting the core electromagnetic laws, including Maxwell's equations, material relations, Ohm's law, and boundary interface conditions, which together establish the physical foundation for modeling electromagnetic fields. To adapt these equations to engineering applications, we introduce relevant quasi-static simplifications and explore their interpretation within the field of electrotechnics. Special attention is given to the potential formulations, including scalar and vector potentials, which enable the development of efficient numerical models for static and dynamic magnetic problems[23].

Building on this theoretical foundation, the chapter then transitions into the finite element implementation using Altair Flux 2D, a professional simulation tool widely used for electromagnetic analysis. This includes the geometrical setup, material definition, circuit modeling, and boundary condition assignment, all tailored to represent a PMSM accurately[24].

The simulation section presents results across four distinct case studies that cover cogging torque computation, back electromotive force (BEMF) analysis, performance evaluation at constant speed, and startup dynamic behavior. Each case demonstrates the power of combining theoretical equations with advanced simulation techniques to yield insights into motor behavior under realistic operating conditions[25].

Finally, the chapter concludes with a critical analysis and discussion of the results, highlighting key observations, trends, and implications for the design and optimization of high-performance electric machines.

2 Physical and Electromagnetic Equations

2.1 B(H) Relation: Magnetic Material Law

This equation describes the relation between the magnetic flux density B and the magnetic field intensity H, depending on the magnetic permeability μ:

$$B = \mu \cdot H \tag{2}$$

Where:

B is the magnetic flux density [T]

H is the magnetic field intensity [A/m]

μ is the magnetic permeability [H/m]

2.2 E(J) Relation: Ohm's Law for Electric Materials

This relation connects the electric field **E** to the current density **J** through the material resistivity ρ:

$$E = \rho \cdot J \tag{3}$$

Where:

E is the electric field [V/m]

J is the current density [A/m^2]

ρ is the resistivity of the material [Ω·m]

3 Electromagnetic Modeling Equations

3.1 Maxwell's Equations (Quasi-static Form)

Ampere's Law (without displacement current):

$$\nabla \times H = J \tag{4}$$

Gauss's Law for Magnetism:

$$\nabla \cdot B = 0 \tag{5}$$

Faraday's Law of Induction:

$$\nabla \times E = -\frac{\partial B}{\partial t} \tag{6}$$

3.2 Magnetostatic Model (Vector Potential Formulation)

Magnetic vector potential A:

$$B = \nabla \times A \tag{7}$$

Governing equation:

$$\nabla \times (1/\mu \cdot \nabla \times A) = J \tag{8}$$

3.3 Magnetodynamic Model

$$\nabla \times (\nu \cdot \nabla \times A) + \sigma \cdot \frac{\partial A}{\partial t} = J_{sour} C_e \tag{9}$$

Where:

$\nu = 1/\mu$ (magnetic reluctivity)

σ is the electrical conductivity

3.4 Electromagnetic Torque (Virtual Work Method)

$$T_{em} = \frac{dW_{C_o}}{d\theta} \tag{10}$$

Or

$$T_{em} = \int v \left(B \cdot \frac{\partial H}{\partial \theta}\right) dV$$

4 Energy and Loss Equations

4.1 Magnetic Energy Density

$$w_m = \frac{1}{2} \cdot B \cdot H \tag{11}$$

4.2 Iron Losses (Simplified Bertotti Model)

$$P_e = k_h \cdot f \cdot B^2 + k_e \cdot f^2 \cdot B^2 \tag{12}$$

Where:

f is the frequency

B is the magnetic flux

k_h, k_e are empirical constants

5 PMSM Electrical Equations in dq Frame

5.1 dq axis Voltage Equations

$$V_d = \mathrm{R_s} \cdot i_d + \frac{d\phi_d}{dt} - \omega \cdot \phi_q \tag{13}$$

$$V_q = \mathrm{R_s} \cdot i_q + \frac{d\phi_q}{dt} + \omega \cdot \phi_d \tag{14}$$

With:

$$\phi_d = L_d \cdot i_d + \phi_m \tag{15}$$

$$\phi_q = L_q \cdot i_q \tag{16}$$

5.2 Electromagnetic Torque Equation in dq Frame

$$\mathrm{T_e} = \left(\frac{3}{2}\right) \cdot \mathrm{p} \cdot (\phi_d \cdot i_q - \phi_q \cdot i_d) \tag{17}$$

Or

$$\mathrm{T_e} = \left(\frac{3}{2}\right) \cdot \mathrm{p} \cdot (\phi_m \cdot i_q + (L_d - L_q) \cdot i_d \cdot i_q)$$

6 Presentation of Altair Flux 2D

Altair Flux 2D is a professional finite element analysis (FEA) software developed for the simulation of low-frequency electromagnetic devices. Based on the finite element method, Flux 2D enables the accurate modeling of magnetic, electric, and thermal behaviors in both steady-state and transient conditions[26].

Originally developed in collaboration with the G2ELab (Laboratory of Electrotechnics in Grenoble) and now distributed by Altair, Flux has become a widely used tool in research and industry for the analysis and design of electrical machines, actuators, sensors, and electromagnetic systems[27].

The software consists of the following key modules:

Preprocessing module: Allows the creation of the geometry, the selection or customization of material properties (via the CLSMAT material library), the assignment of physical properties to regions (PROPHY), the definition of electric circuits (CIRFLU), and the automatic meshing of 2D geometries.

Solver module: Performs the numerical computation of electromagnetic or thermal fields using various modeling approaches suited for a range of engineering problems.

Post-processing module: Offers tools for visualizing results through field lines, potential maps, and curve plots. It also calculates global quantities such as electromagnetic torque, magnetic flux, inductance, and forces along defined paths.

Thanks to its open environment, Flux 2D can be integrated with other tools within the Altair ecosystem, such as HyperStudy, which will be used in the third part of this work to perform optimization processes. This integration makes it an ideal solution for multi-variable optimization and design exploration[28].

6.1 Implementation of the Finite Element Model using Altair Flux 2D

The implementation of the Finite Element (FE) model using Altair Flux 2D refers to the process of creating, configuring, and solving a multiphysics simulation environment where electromagnetic behavior is analyzed through the finite element method. Altair Flux 2D is a powerful software tool developed by Altair Engineering for simulating low-frequency electromagnetic devices, such as electric machines, transformers, and sensors.

This implementation involves several stages, including:

Preprocessing: Defining the geometry of the system, assigning material properties, setting up boundary conditions, and generating the mesh.

Solving: Using Altair's FE solver to calculate the electromagnetic fields under various operating conditions.

Postprocessing: Visualizing field distributions and extracting key performance indicators such as torque, losses, or magnetic flux density.

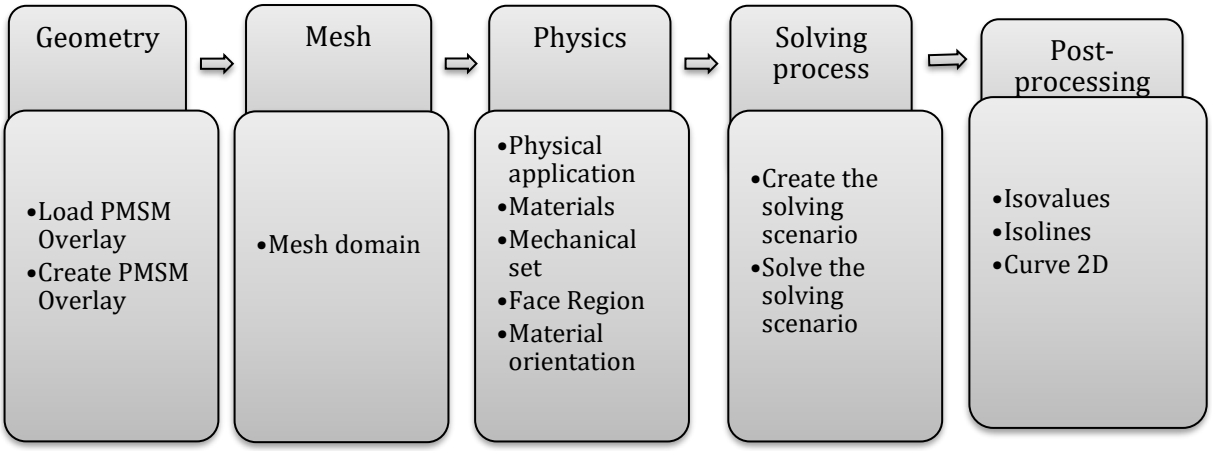

Figure 9: General Approach for Implementing the Model in Flux

6.2 Geometrical Description

The geometrical description phase represents the first step in the process of implementing the mathematical model of the machine under study. Before building the model and its geometry in the simulation environment, it is necessary to define the different components of the problem as well as their associated physical parameters.

This preliminary stage helps ensure a clear structural understanding of the system and determines the configuration of parts such as the rotor, stator, magnets, windings, and airgap. Each region must be properly sized and located,

as this will affect the accuracy of the mesh and the reliability of the simulation results.

The geometrical model is then created in Altair Flux 2D, either using built-in CAD tools or by importing geometry, to faithfully represent the structure and operating conditions of the electrical machine.

7 Simulation Results in FLUX 2D

7.1 Geometry

This section describes the geometry and meshing of the modeled motor in a simplified manner.

The user must have a solid understanding of all preprocessing features available in FLUX, as illustrated in Figure 10.

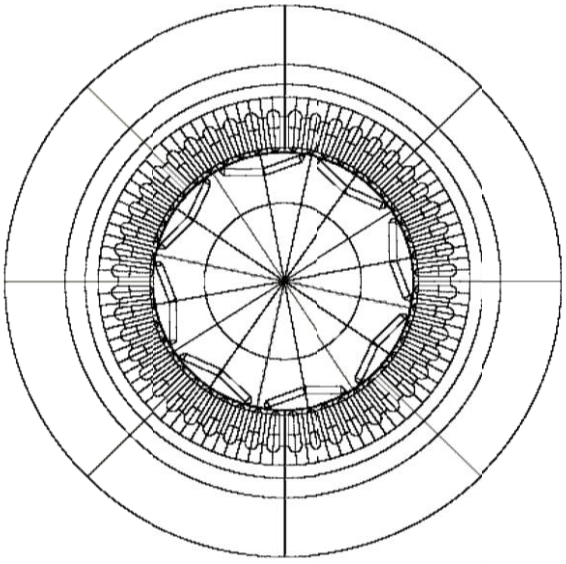

Figure 10: shows the 2D geometric representation of the MSAP machine in FLUX

Table 4: Presents the key geometrical parameters used in the simulation

	Parameters	Valeurs
machine	Max bus voltage	500 v
	Peak torque	400 N.m
	Max speed	6000 rpm
	Peak power rating	50 kW at 1200-1500 rpm
general	Length Unit *	Millimètre
	Mesh Density	0.5
	Inner radius	110
	Outer radius	140
	With shaft	Yes
gap	Airgap (GAP)	0.6
	Excentricities and Periodicities	Without excentricity
	Use Periodicities	Yes
	Rotating Airgap	Two layers airgap
rotor	Magnet shape	Rotoripm
	Shaft radius (RadSH-1)	56
	Thickness of magnet (LM) "	5
	Magnet pole arc (BetaM) [Deg] "	140
	Number of magnets blocks per pole (Nmbp)*	1
	Number of poles (POLES) *	8
	Rotor external radius (rad1) =	92
	Rotor shift angle (RotorAng)[Deg] *	0.0
Magent	magnet type	Type4
	(Web)	10
	Magnet Width per pole (MagWid)	54
	Bridge	1.0
	Depth of pole cap (ipmHq)*	10
	Radial web length (IWeb) =	2.75
	Width of gutter or slot inboard of magnets (gutter)	0.0
	Hub width (d0)	24.0
	Magnet inset (inset) *	0.0
Stator	LamShap	Circle
	Stator outer radius (RAD3)	141.0
	Slot shape	StatorRound
	Slot opening (SO)*	2.0
	Radial depth (TGD) *	1.0
	Slot depth	30.0
	Tooth width stator (TWS) *	6.5
	Slot Opening angle (SOANG) [Deg] *	40
	Tooth fillet radius near stator slot opening (FILSO)	1.0

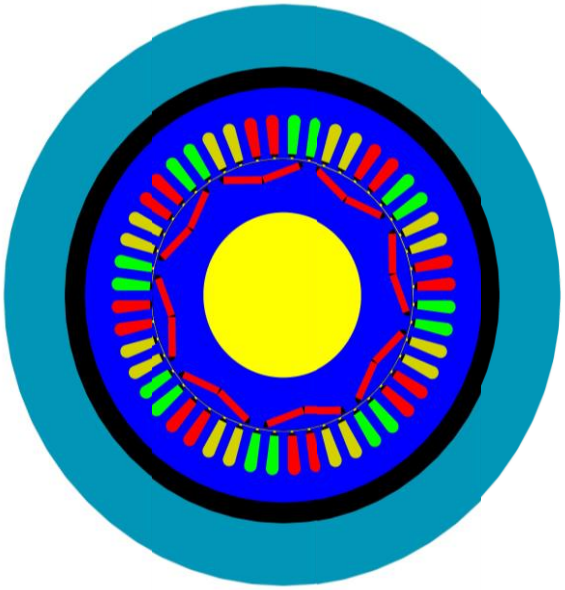

Figure 11: Illustrates how surface regions were assigned

Table 5: Material and Region Definitions for IPMSM Finite Element Model

Volume Region Name	Type of Region	Material	Mechanical Set
INFINITE	Air or vacuum region	-	STATOR
PHASE_NEG_3	Air or vacuum region	-	STATOR
PHASE_POS_1	Air or vacuum region	-	STATOR
PHASE_POS_2	Air or vacuum region	-	STATOR
PRESLOT	Air or vacuum region	-	STATOR
ROTATING_AIRGAP	Air or vacuum region	-	STATOR
MAGNET1_1_POLE_1	Magnetic non-conducting region	CY_N35_20DEG(NdFeB)	ROTOR
MAGNET2_1_POLE_1	Magnetic non-conducting region	CY_N35_20DEG(NdFeB)	ROTOR
ROTOR_AIR	Air or vacuum region	-	ROTOR
SHAFT	Air or vacuum region	-	ROTOR
ROTOR	Laminated magnetic non-conducting region	COGENT_M270_35A_50HZ (with 0.97 stacking factor)	ROTOR
STATOR	Laminated	COGENT_M270_35A_50HZ	STATOR

	magnetic non-conducting region	(with 0.97 stacking factor)	
STATOR_AIR	Air or vacuum region	-	STATOR
WEDGE	Air or vacuum region	-	STATOR

7.2 Material Creation

Permanent magnets are made of NdFeB (Neodymium Iron Boron). Table 6 and 7 lists the magnetic properties of the model used: NdFeB permanent magnets.

Table 6: B(H) Linear Magnet – Defined in Br Model

Name	Remanent Flux Density (T)	Relative Permeability (μr)
NDFEB	1.2	1.05

Table 7: J(E) Electrical Property – Isotropic Resistivity

Name	Resistivity (Ω·m)
NDFEB	1.4×10^{-6}

7.3 Circuit Creation

To represent the motor accurately, it is important to consider end effects, including the inductance and resistance of coil heads and short-circuit rings.

The electrical circuit (Figure III.27) includes:

- Current sources : I_1, I_2, I_3.
- Stranded coil conductors: C_1, C_2, C_3.
- Leakage inductances : L_1, L_2, L_3.
- Voltage drop resistances : R_1, R_2, R_3, R_4, R_5, R_6.
- Solid conductors (Magnets) : M1,M2.

Table 8 : Mesh Elements Summary

Mesh Element	Count / Percentage
Nodes	16,828
Line elements	1,731
Surface elements	8,118
Unevaluated elements	0%
Excellent quality elements	97.51%
Good quality elements	1.59%
Average quality elements	0.85%
Low quality elements	0.05%

The mesh used for the simulation consists of 16,828 nodes, 1,731 line elements, and 8,118 surface elements, which indicates a relatively detailed and dense mesh—suitable for accurately capturing the electromagnetic behavior of the IPMSM.

Importantly, 0% of the elements are unevaluated, meaning the meshing algorithm successfully assessed the quality of all elements, which is a strong indicator of a clean and complete model setup.

Regarding element quality:

97.51% of the elements are of excellent quality, which ensures very high accuracy in the numerical simulation and minimizes the risk of convergence or stability issues.

1.59% of the elements are of good quality, still acceptable for finite element analysis (FEA), and will not significantly impact the results.

Only 0.85% are of average quality and 0.05% are of low quality, which is negligible and unlikely to affect the overall accuracy of the simulation. However, these elements could be monitored in future refinements, especially if the analysis is extended to thermal or structural domains.

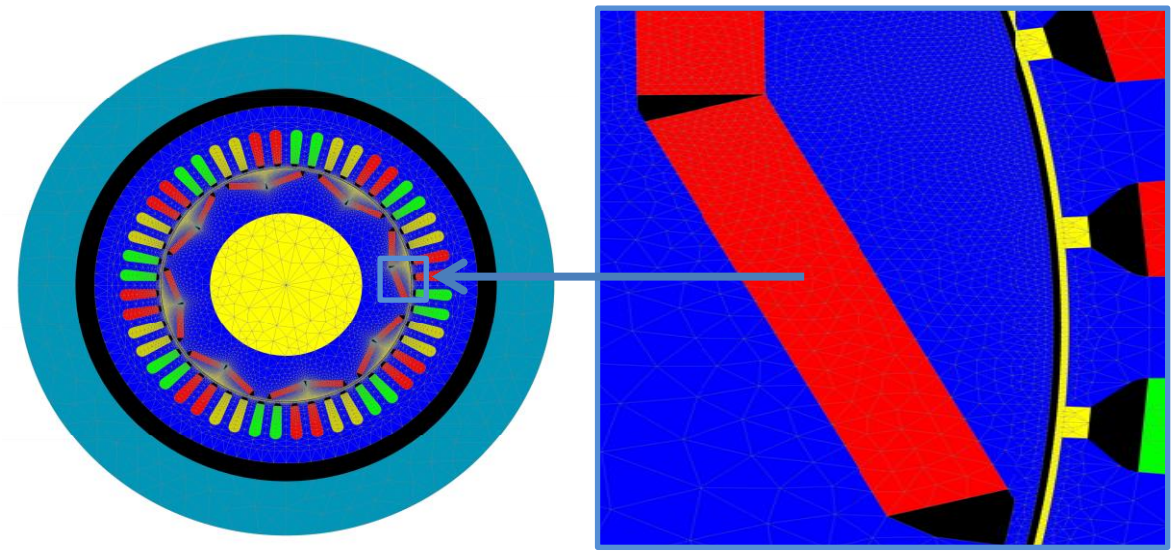

Figure 12: Mesh Representation

8 Results from 2D Flux Simulation for four cases

This section presents several simulation cases to evaluate the performance of the IPMSM motor, including the computation of cogging torque, the analysis of back electromotive force (BEMF), the assessment of performance at constant speed, and the simulation of dynamic behavior during startup.

8.1 Case one computation of the cogging torque

The cogging torque is computed with a multi-position simulation and no current. The multi-position is simulated with a transient application at constant speed. The speed is chosen to be 1/6 rpm which corresponds to 1 mechanical degree per second.

8.2 Overview of Output Curves

8.2.1 Setting Up a Solve Scenario

Table 9 : Parameters of solving-caseone

Parameter	Value
Name	Cogging
Control Type	Control by Mechanical Set
Controlled Position	Rotor
Rotation Interval	
Lower Limit	0.0°
Upper Limit	7.5°
Step Value	0.1875°

8.2.2 Graphical results of Isovalues of the magnetic flux density and flux isolines on surface regions

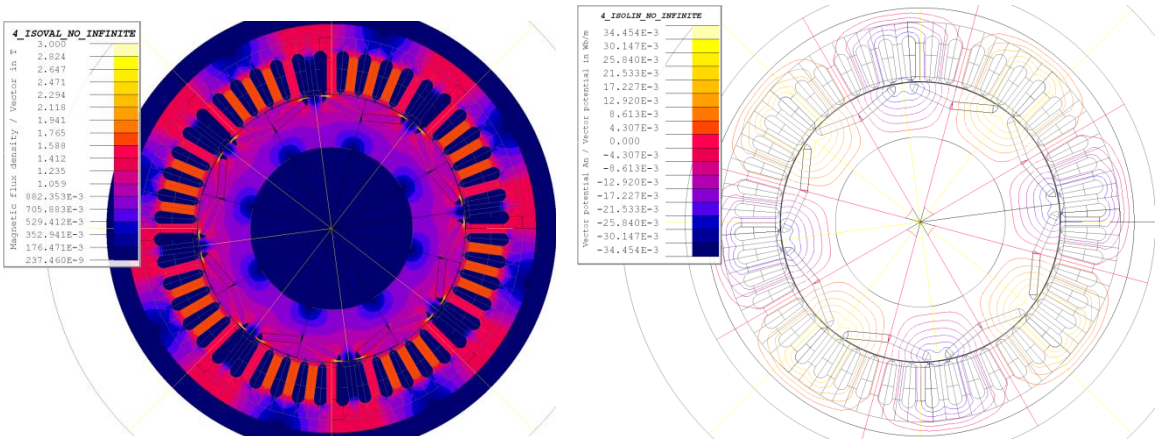

(a) (b)

Figure 13: Graphical results : (a) Isovalues of the magnetic flux density on surface regions, (b) flux isolines on surface regions

8.2.3 Output Curves

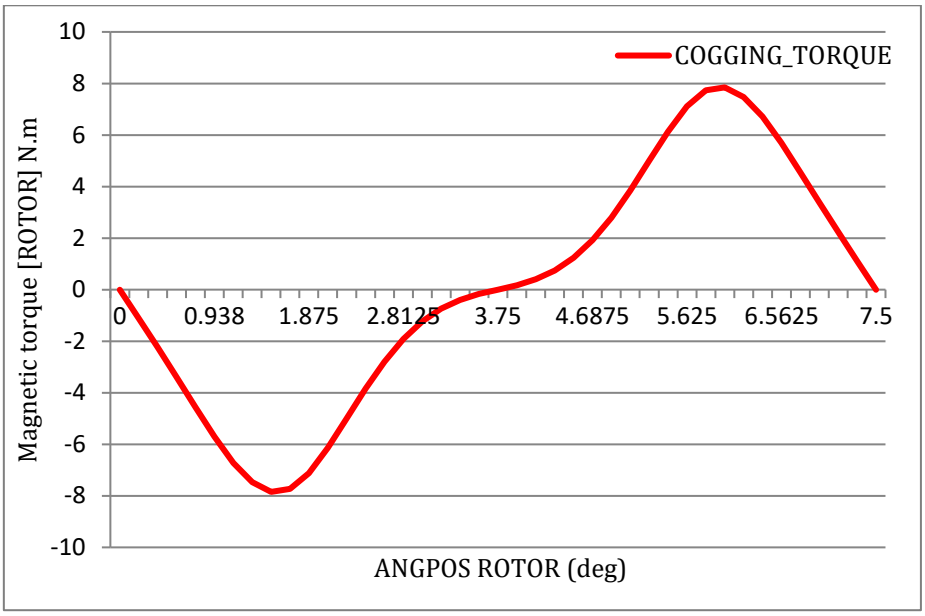

Figure 14: Variation of torque as a Function of Angle

8.3 Case two back electromotive force (bemf) computation

The back electromotive force EMF is computed with the speed of 1000 rpm and external circuit connections.

It corresponds to the motor being in generator mode at no load. The computed back EMF allows determining the current control angle.

8.3.1 Creating coupling electric circuit

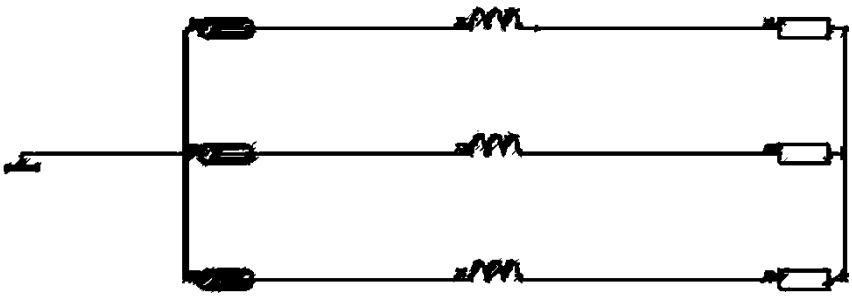

Figure 15 : electric circuit of case two

8.3.2 Parameters of Components in the Electric Circuit

Table 10 : Parameters of Coils Conductors, Inductors, Resistors

Parameter	Value
coil conductors : C_1, C_2, C_3	0.088
inductors : L_1, L_2, L_3	0.15E-3
resistors : R_1, R_2, R_3	1E-4

8.3.3 Overview of Output Curves

8.3.3.1 Setting Up a Solve Scenario

Table 11 : Parameters of solving-case two

Parameter	Value
Name	BACK_EMF
Control Type	Control by Mechanical Set
Controlled Position	Rotor
Rotation Interval	
Lower Limit	0.0°
Upper Limit	90°
Step Value	0.5°

8.3.3.2 Graphical results of Isovalues of the magnetic flux density and flux isolines on surface regions

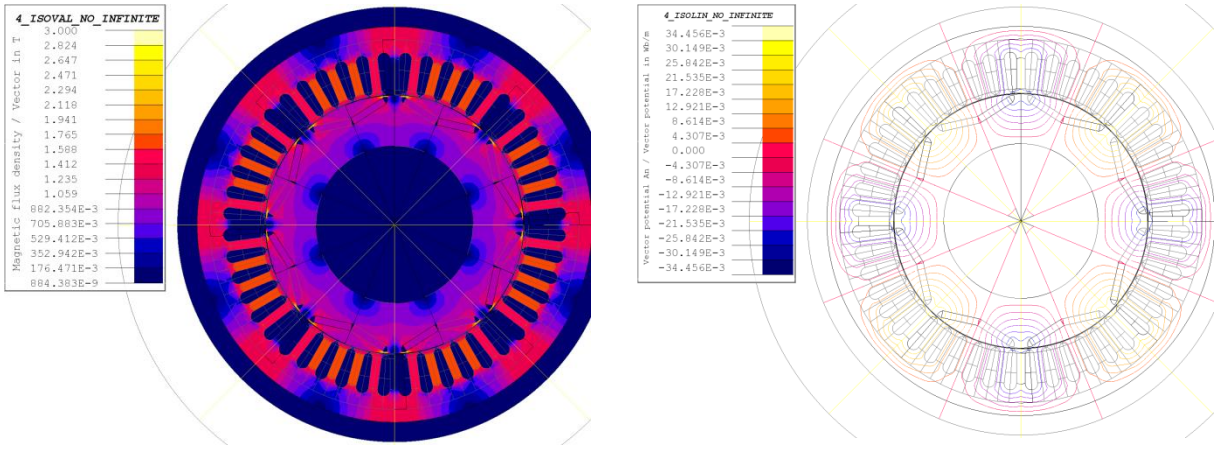

(a) (b)

Figure 16: Graphical results : (a) Isovalues of the magnetic flux density on surface regions, (b) flux isolines on surface regions

8.3.3.3 Output Curves

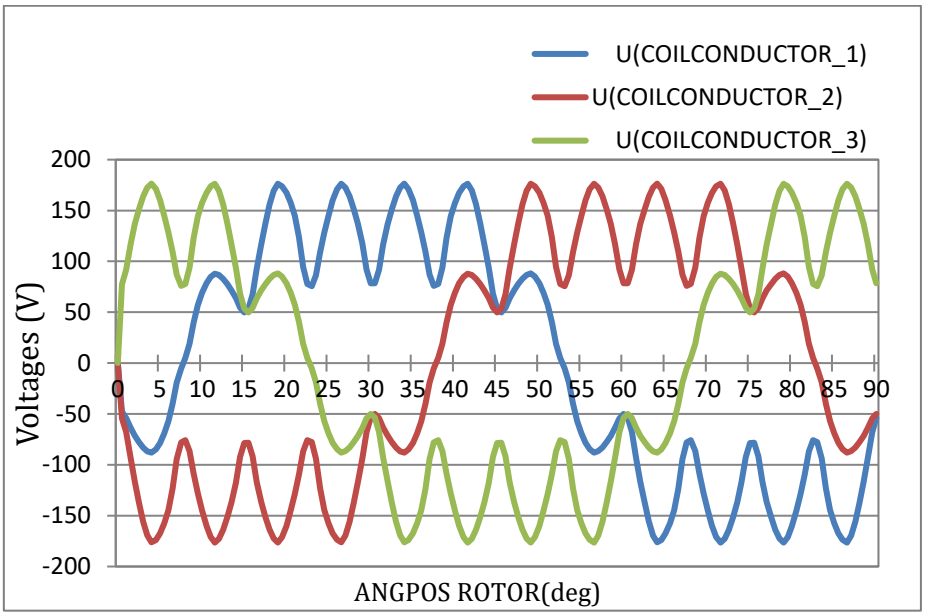

Figure 17: the voltage through coil conductors

8.4 Case three performances at constant speed

The motor is driven with a 3 phase sine current and running at constant speed.

The simulated motor performances are used to compute shaft torque, torque ripples, core losses (Bertotti and LS model) and efficiencies.

8.4.1 Creating new I/O parameters

Table 12: I/O parameters of case three

Parameter Name	Type of Parameter	Expression / Reference Value
GAMMA	Parameter defined by a formula	45
MAX_CURRENT	Parameter defined by a formula	200
SPEED	Parameter controlled via a scenario	1200
FREQUENCY	Parameter defined by a formula	SPEED / 60 × POLES / 2
OMEGA	Parameter defined by a formula	2 × Pi × FREQUENCY

8.4.2 Creating coupling electric circuit

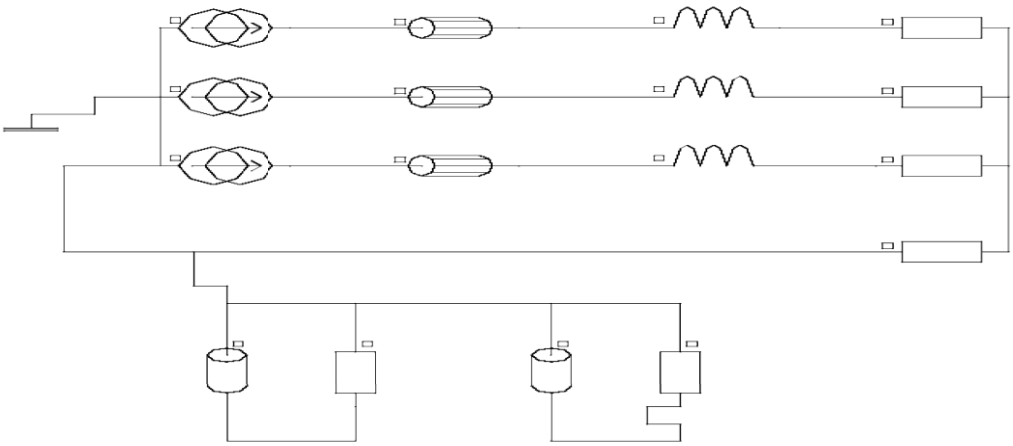

Figure 18 : Shows the complete integrated circuit in the FLUX project

8.4.3 Parameters of Components in the Electric Circuit

This section presents the main electrical parameters of the components used in the simulation circuit. It includes coils, conductors, inductors, resistors, and current sources, all of which play a key role in the system's behavior.

Table 13 : Parameters of Coils Conductors, Inductors, Resistors Current

Component Type	Component(s)	Value / Expression
Coils (Conductors)	C_1, C_2, C_3	0.088
Inductors	L_1, L_2, L_3	0.15×10^{-3} H
Resistors	R_1, R_2, R_3	1×10^{-4} Ω
Resistors	R_4, R_5, R_6	1×10^{4} Ω
Current Source I_1	Phase A	MAX_CURRENT*Sin(OMEGA*TIME+GAMMA*PI()/180)
Current Source I_2	Phase B	MAX_CURRENT*Sin(OMEGA*TIME+GAMMA*PI()/180-2*PI()/3)
Current Source I_3	Phase C	MAX_CURRENT*Sin(OMEGA*TIME+GAMMA*PI()/180-4*PI()/3)

8.4.4 Overview of Output Curves

8.4.4.1 Setting Up a Solve Scenario

Table 14 : Parameters of solving-case three

Parameter	Value
Name	CST_SPEED
Control Type	Control by Mechanical Set
Controlled Position	Rotor
Rotation Interval	
Lower Limit	0.0°
Upper Limit	92°
Step Value	1°

8.4.4.2 Graphical results of Isovalues of the magnetic flux density and flux isolines on surface regions

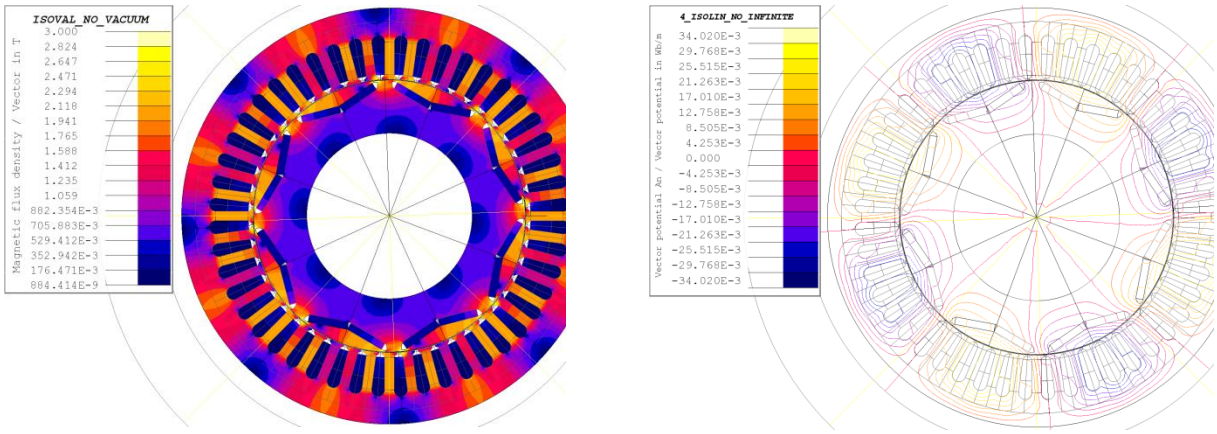

(a) (b)

Figure 19: Graphical results : (a) Isovalues of the magnetic flux density on surface regions, (b) flux isolines on surface regions

8.4.4.3 Output Curves

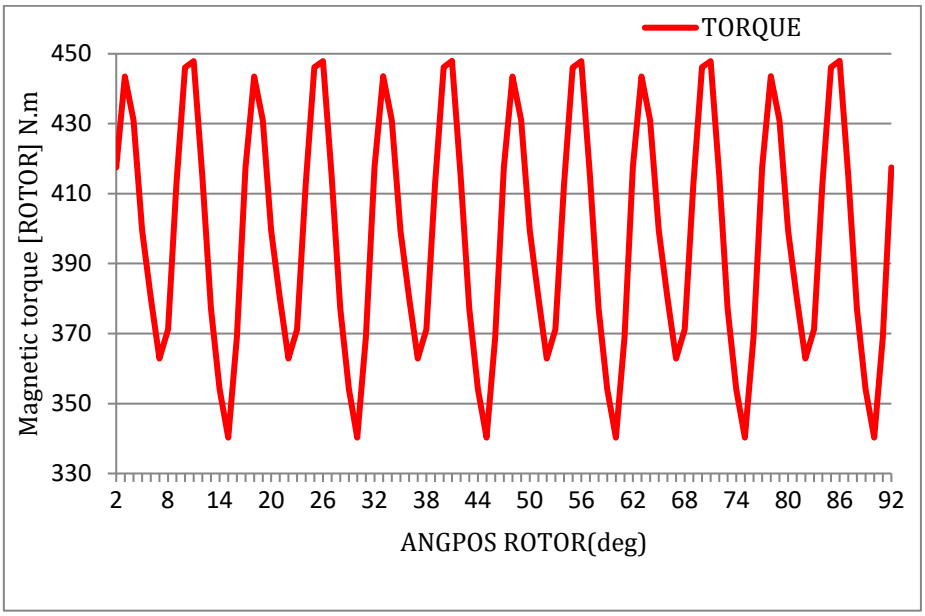

Figure 20 : Variation of torque as a Function of Angle

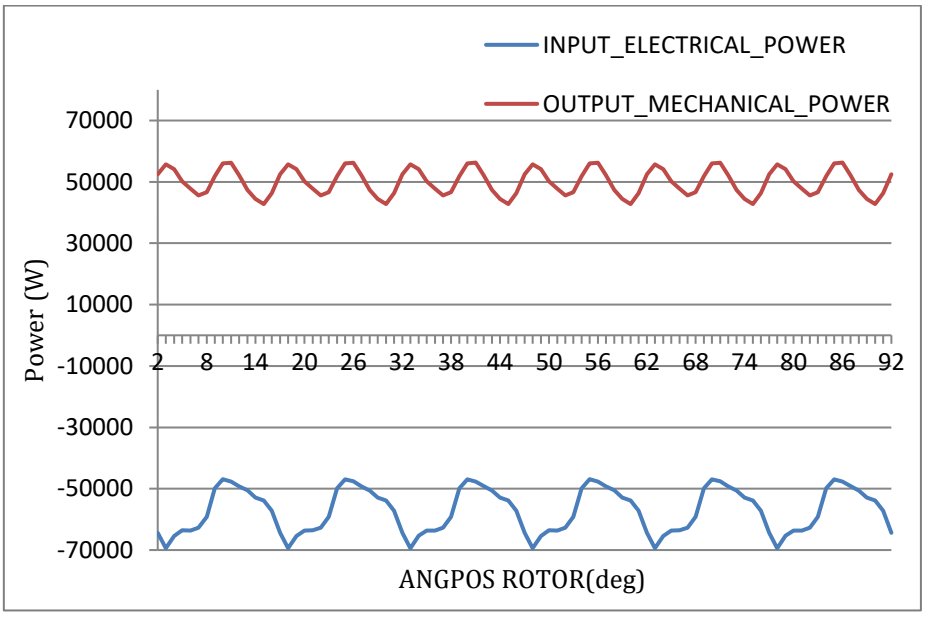

Figure 21 : Variation of power as a function of angle

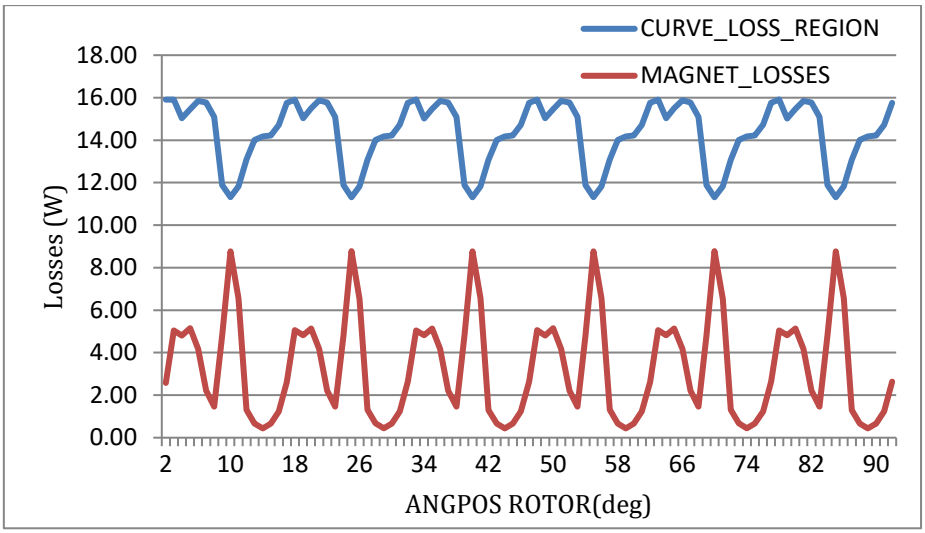

Figure 22 : Variation of loss region and magnet losses as a function of angle

8.5 Case four Startup dynamic behavior

The dynamic behavior of the motor during start up is simulated with a proposed current control strategy.

The winding is supplied in current depending on the rotor position.

Electric circuit it is the same circuit previous case with different parameters.

8.5.1 Parameters of Components in the Electric Circuit

Parameters of Coils Conductors, Inductors and Resistors it is the same previous case and parameters of Current.

Table 15 : Parameters of current

Component Type	Component	Value / Expression
Current Source I_1	Phase A	MAX_CURRENT*Sin(((AngPos(ROTOR)-7.5)*POLES/2+GAMMA)*Pi()/180-0*Pi()/3)
Current Source I_2	Phase B	MAX_CURRENT*Sin(((AngPos(ROTOR)-7.5)*POLES/2+GAMMA)*Pi()/180-2*Pi()/3)
Current Source I_3	Phase C	MAX_CURRENT*Sin(((AngPos(ROTOR)-7.5)*POLES/2+GAMMA)*Pi()/180-4*Pi()/3)

8.5.2 Overview of Output Curves

8.5.2.1 Setting Up a Solve Scenario

Table 16 : Parameters of solving-case four

Parameter	Value
Name	STARTING
Control Type	Time
Rotation Interval	
Lower Limit	0.0
Upper Limit	0.08
Step Value	0.001

8.5.2.2 Graphical results of Isovalues of the magnetic flux density and flux isolines on surface regions

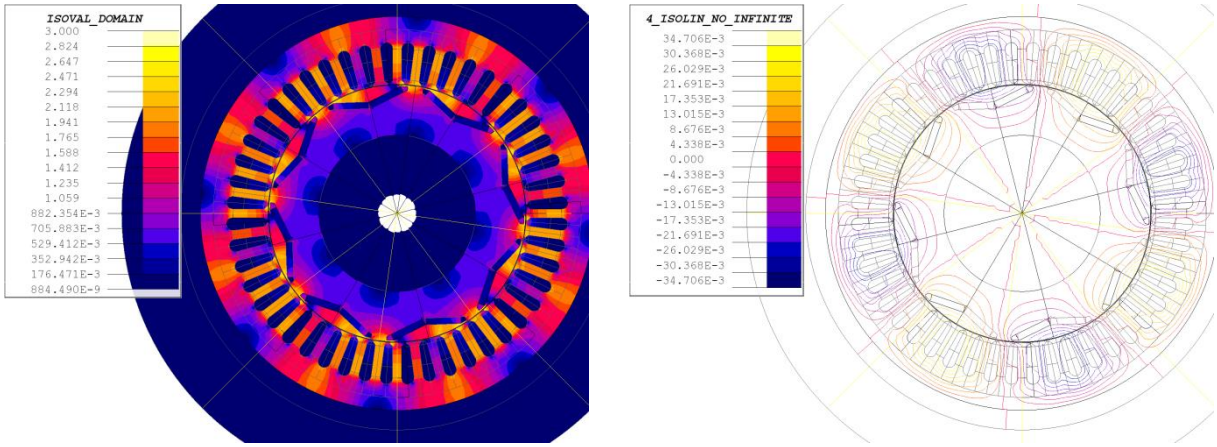

(a) (b)

Figure 23 Graphical results : (a) Isovalues of the magnetic flux density on surface regions, (b) flux isolines on surface regions

8.5.2.3 Output Curves

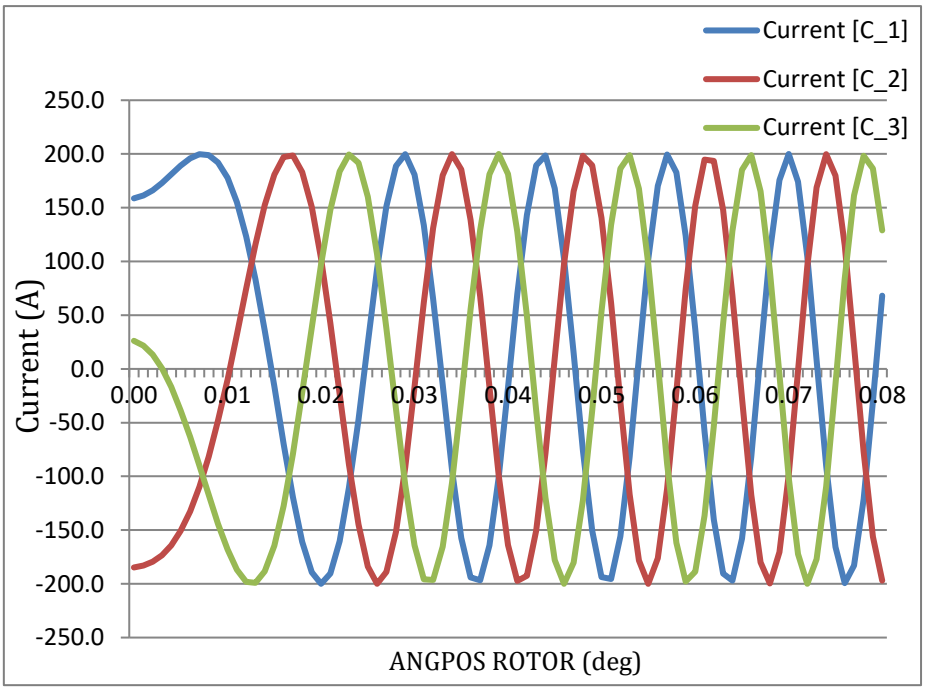

Figure 24 : Variation of current as a Function of Angle

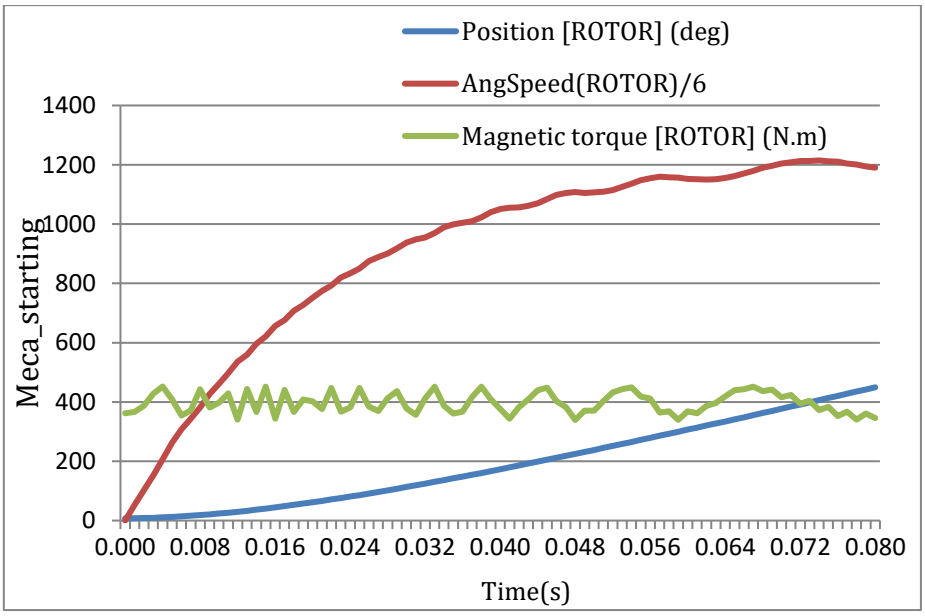

Figure 25 : Variation of Position, AngSpeed and Magnetic torque of rotor as a Function of Time

9 Anyalis of results

Prior to initiating the optimization process, the baseline configuration of the motor was assessed through two critical simulation cases: torque versus rotor angle (Case 1) and three-phase voltage waveform analysis (Case 2). The results from these initial cases revealed several performance limitations that warranted further investigation.

In Case 1, the torque-angle curve exhibited significant irregularities and pronounced fluctuations, indicating unstable torque behavior. These irregularities were attributed to an asymmetric distribution of the magnetic flux and localized magnetic saturation within the motor structure. Such conditions are known to induce elevated torque ripple, increase mechanical stress, and degrade overall torque production efficiency.

In Case 2, the three-phase voltage waveforms demonstrated a noticeable imbalance and distortion, with visible harmonic content. This distorted back-electromotive force (back-EMF) profile suggested suboptimal magnetic circuit design or winding arrangement. Consequently, these deficiencies could lead to reduced motor efficiency and heightened stress on the inverter system, especially under dynamic operating conditions.

To further investigate the baseline motor behavior, Cases 3 and 4 were analyzed, representing constant-speed and dynamic startup conditions, respectively. The simulation outcomes revealed that the electromagnetic characteristics in both cases were remarkably similar. The average torque values differed by less than 0.1%, indicating a stable motor response under varying load conditions.

Notably, Case 4—corresponding to the dynamic operation—demonstrated a reduction in torque ripple of approximately 4% compared to Case 3. This reduction is considered a positive indicator of smoother startup behavior. However, the torque ripple values remained relatively high overall, underscoring the need for targeted reduction strategies during subsequent optimization phases.

The motor's initial design achieved about 87.5% efficiency, confirming good energy conversion. Iron and magnet losses were very low (0.2% and 0.05% of input power). The current waveform showed a nearly balanced system, with slight phase differences due to electrical angle shifts. The rotational speed was slightly under the nominal value because of transient loading. Overall, the motor's pre-optimization state performed well but showed torque ripple and minor losses, indicating room for further optimization in Chapter Three.

10 Conclusion

This chapter presented a comprehensive simulation study of an Interior Permanent Magnet Synchronous Motor (IPMSM) using Altair Flux 2D. Through a series of structured cases, we examined various performance aspects of the motor, including cogging torque, back electromotive force (BEMF), behavior at constant speed, and dynamic response during startup. Each simulation provided valuable insight into how design parameters influence motor behavior under different operating conditions.

The use of Flux 2D enabled accurate modeling and visualization of the electromagnetic behavior, helping to assess the efficiency and functionality of the motor under realistic scenarios. These results form an essential foundation for further improvement and validation.

In the following chapter, the focus shifts to the optimization process, where the goal is to improve key performance indicators of the motor. We will apply optimization techniques to Case Three (constant speed performance) and Case Four (startup behavior) using HyperStudy, aiming to identify the most efficient configurations within the defined design space. This marks the transition from simulation to intelligent optimization, paving the way for enhanced motor performance in practical applications.

Chapter 3 Optimization of the Magnets

1 Introduction

In the context of modern electrical machine design, achieving high-performance and cost-effective solutions demands the use of advanced optimization tools. This project employs Altair HyperStudy™, a powerful platform for multidisciplinary design exploration and optimization, to improve the performance of an Interior Permanent Magnet Synchronous Motor (IPMSM)[29]. HyperStudy was selected due to its compatibility with Altair's simulation tools like Flux and FluxMotor, as well as its support for both surrogate model-based and direct optimization strategies. The main goal of this study is to optimize key rotor parameters to reduce magnet volume and torque ripple while maintaining sufficient torque output. By integrating Flux 2D simulations with HyperStudy's optimization workflows, a comprehensive design exploration was conducted, resulting in several high-performing rotor configurations[30].

2 Choosing the Optimization Tool

2.1 Why HyperStudy Was Selected

Altair HyperStudy™ was chosen as the optimization tool in this project due to its robust and advanced capabilities in multi-disciplinary design exploration and optimization. It enables engineers to analyze, predict, and improve the performance and reliability of their models using a wide range of state-of-the-art mathematical algorithms and data mining techniques[31].

HyperStudy offers seamless integration with Altair tools such as Flux and FluxMotor, making it ideal for electromagnetic system design. It also supports shape optimization and automatic process workflows, allowing for easy exploration of the design space[32].

2.2 Introduction to HyperStudy

HyperStudy is advanced design optimization software developed by Altair. It provides:

Tools for Design of Experiments (DOE) to understand how input parameters affect performance.

Predictive modeling to reduce computational effort by approximating simulation results.

A library of optimization algorithms like GRSM (Global Response Surface Method), SQP, and Genetic Algorithms.

Features for robustness and reliability analysis through stochastic studies.

Powerful post-processing tools such as Pareto plots, correlation matrices, and histograms.

Integration with both Altair and third-party tools for a flexible simulation workflow[33].

3 Optimization Strategy

Two optimization workflow are available in HyperStudy

3.1 Optimization Based on Fit Functions

This method uses mathematical models, called *fit functions*, to approximate the behavior of a system. Instead of running time-consuming simulations each time, the optimization algorithm uses these simpler functions to quickly predict outputs based on inputs[34].

Fit functions are usually built using data from previous simulations (design of experiments), and they allow faster exploration of the design space and easier identification of optimal solutions[35].

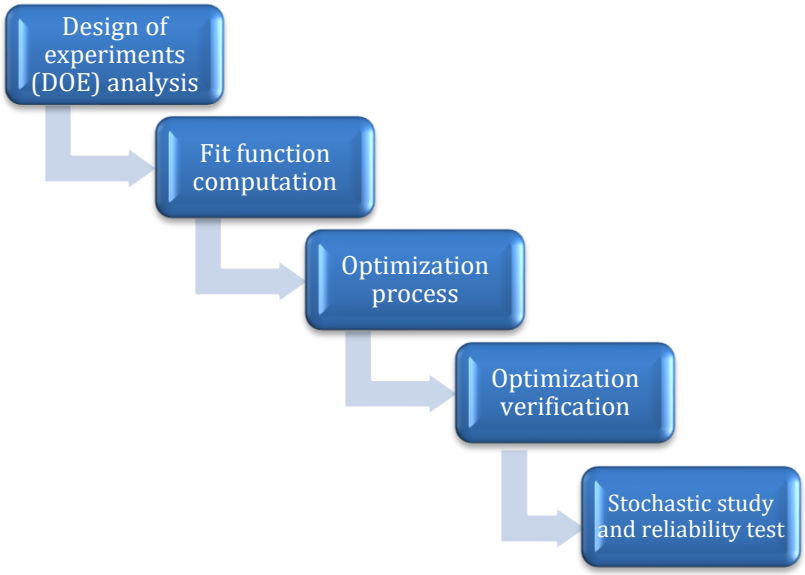

Figure 26 : optimization Based on Fit Functions method

3.2 Direct Optimization Method

The Direct Optimization Method is a technique that searches for the best solution by directly evaluating the objective function without using gradient information. It is especially useful when the objective function is complex, noisy, or non-differentiable[22].

3.2.1 Key Characteristics

These methods do not rely on gradient information, making them well-suited for solving nonlinear, black-box, or simulation-driven optimization problems. Common algorithms include[36-40]:

- Genetic Algorithms (GA)
- Particle Swarm Optimization (PSO)
- Nelder-Mead Simplex
- Simulated Annealing
- GRSM (Global Response Surface Method)

3.2.2 Applications

3.2.2.1 Engineering Design Optimization

Gradient-free optimization methods are widely used in engineering design problems, where the objective functions are often non-linear, discontinuous, or expensive to evaluate through simulations. These methods allow engineers to explore a wide design space and identify optimal configurations without requiring explicit derivative information[35].

3.2.2.2 Control System Tuning

In complex control systems, especially those involving nonlinear dynamics or time delays, traditional gradient-based tuning may not be feasible. Gradient-free methods provide a practical alternative by optimizing control parameters based on performance metrics obtained from simulations or real-world feedback[41].

3.2.2.3 Machine Learning Model Selection

Selecting the best hyperparameters or model structures in machine learning can be framed as an optimization problem. Gradient-free techniques like random search or Bayesian optimization are commonly used when gradients are not available or unreliable, especially in non-differentiable models[42].

3.2.2.4 Multi-Objective Optimization

Many real-world problems involve optimizing several conflicting objectives simultaneously. Gradient-free algorithms, particularly evolutionary approaches, are highly effective in exploring trade-offs and generating a Pareto-optimal front, making

them ideal for multi-objective optimization scenarios in fields like automotive design, energy systems, and robotics[43].

4 Optimization Setup

4.1 Method slacet for Optimization

Type of optimization is Direct Optimization.

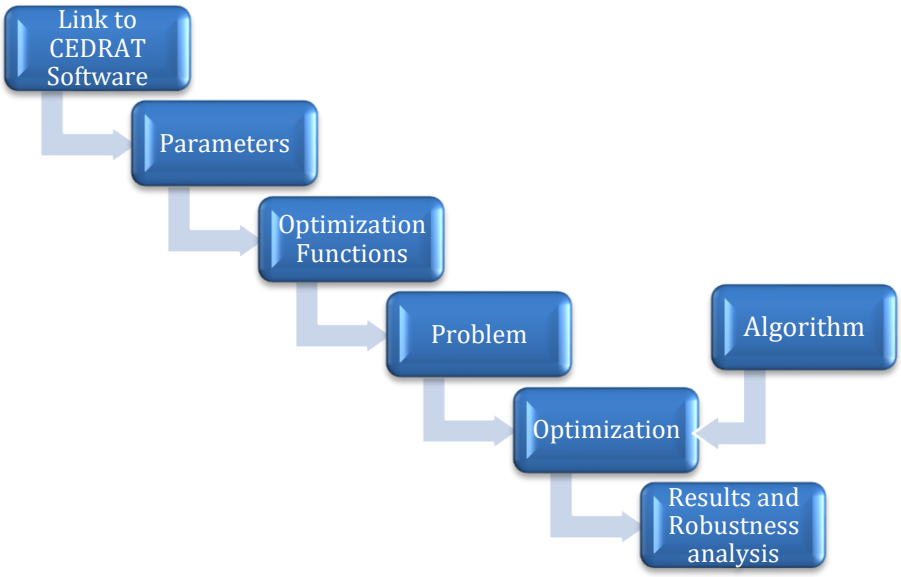

Figure 27 : Direct Optimization method

4.2 Pre-Optimization Setup in Flux 2D for HyperStudy Integration

Before starting the optimization process in HyperStudy, it is necessary to create a Python script inside the Flux project. This script is responsible for automatically exporting the torque values after each simulation run. These torque values are extracted from the simulation results using macros such as "`Analyse2DCurve`"and "`CreateIOTabulatedParameterFrom2DCurve`"[44] .

The script ensures that HyperStudy receives the correct output response for each design configuration. This step is essential for linking the physical simulation with the optimization engine and allows the creation of a fully automated design exploration workflow[45].

4.3 Parameters

4.3.1 Design Variables

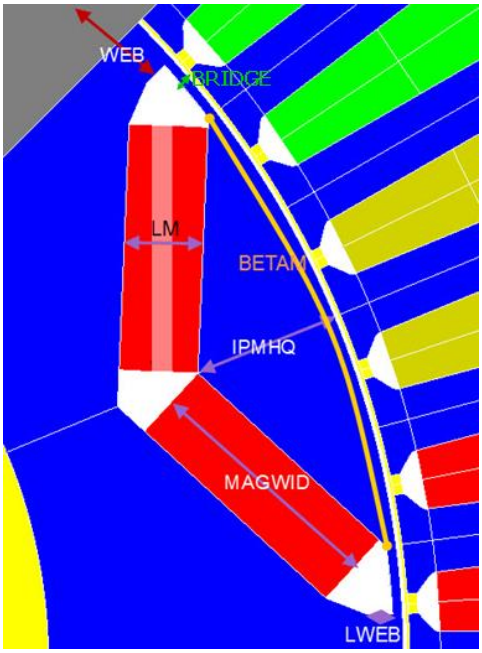

Figure 28 : Design Variables

Table 17 : Input Design Parameters for the IPM Rotor Model

Parameter	Value	Unit	Description
BETAM	140	deg°	Magnet angle (insertion or orientation angle)
BRIDGE	1	mm	Thickness of the rotor iron bridge
IPMHQ	10	mm	Height of the internal PM slot
LM	5	mm	Length of the magnet
LWEB	2.75	mm	Width/length of lower web
MAGWID	54	mm	Width of the magnet
WEB	10	mm	Thickness of supporting rotor web

4.3.2 **Responses**

4.3.2.1 Torque Export Process

Exported torque values:

- Mean Torque (average over rotor angle sweep)
- Maximum Torque
- Minimum Torque

Table 18 : Parameter torque values

Parameter	Value	Unit
Torque_ Mean	397.34324	Nm
Torque_ Max	447.97486	Nm
Torque_ Min	340.25173	Nm

4.4 Objective Function

Minimize magnet area

Formula: Magnet area = LM × MAGWID = 5 * 54 =270 mm^2

Minimize Ripple torque

Formula : Ripple torque = ELTORQ_ROTOR_MAX − ELTORQ_ROTOR_MIN

=447.97486-340.25173

Ripple torque =107.72313 Nm

4.5 Constraints

Constraint of Torque_ Mean ≥ 397 Nm

Table 19 : Define output responses in HyperStady

Label	Varname	Expression	Value	Goal Type	Target
ELTORQ_ROTOR_MAX	r_1	m_1.ELTORQ_ROTOR_MAX	447.97486	-	-
ELTORQ_ROTOR_MEAN	r_2	m_1.ELTORQ_ROTOR_MEAN	397.34324	Constraint	≥ 397
ELTORQ_ROTOR_MIN	r_3	m_1.ELTORQ_ROTOR_MIN	340.25173	-	-
Magnet_area	r_4	var_8 (area of magnet)	270.00000	Minimize	-
Ripple_Torque	r_5	r_1 - r_3	107.72313	Minimize	-

4.6 Algorithm

4.6.1.1 GRSM – Global Response Surface Method

GRSM is an optimization algorithm that builds a global response surface (a mathematical model) based on simulation or experimental data. It estimates the relationship between input parameters and performance outputs. The algorithm then searches this surface to find the best design[46].

4.6.1.2 Algorithm Parameters

Table 20 : step of specifications for algorithm method

Parameter	Value
Number of Evaluations	3000
On Failed Evaluation	Ignore failed evaluations
Initial Sampling Points	9
Random Seed	1
Points per Iteration	2
Max Failed Evaluations	20000
Stop after no Improvement	1000
Enhance Efficiency	Not listed
Inclusion Treatment	with initial sampling

4.7 Optimization Results

4.7.1 Evaluate

The HyperStudy optimization process initially generated 5,758 geometric configurations. From these, 3,000 designs were selected for detailed analysis. Ultimately, 19 optimal geometric designs were identified as the best-performing solutions.

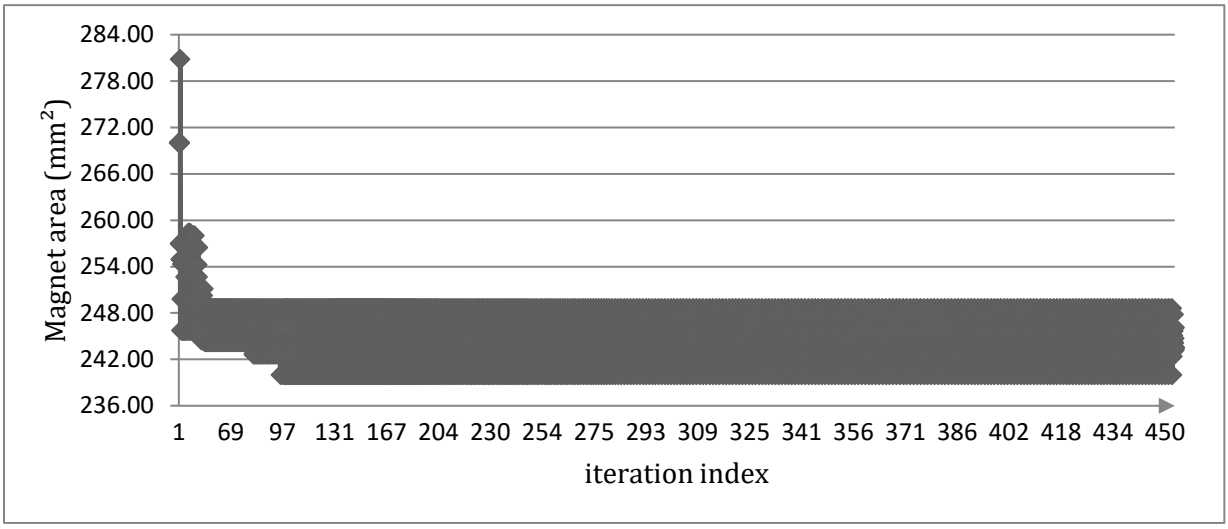

(a)

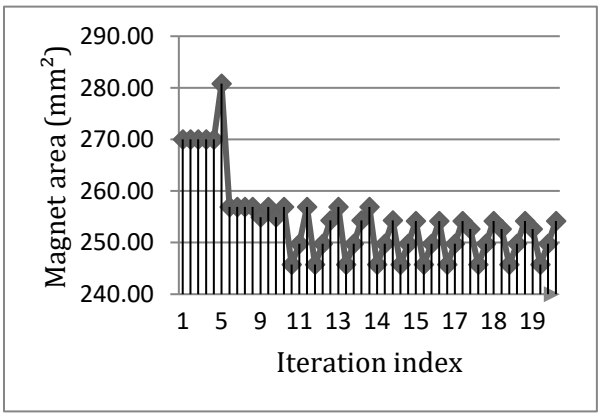

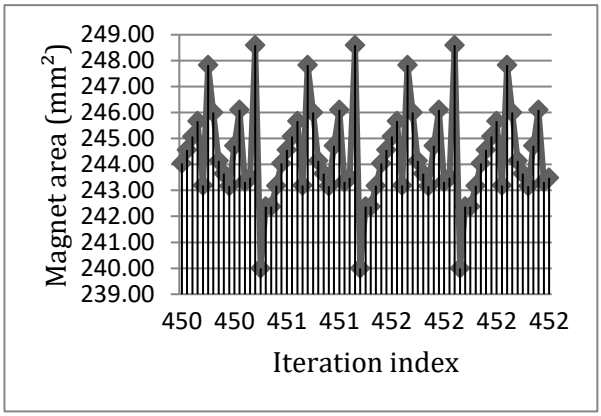

(b) (c)

Figure 29 : Iteration Plot : (a) Objective Function During Magnet Area Optimization, (b) Iterations 1–20 from the Original Iteration Plot of Magnet Area Optimization , (c) Iterations 450–452 from the Original Iteration Plot of Magnet Area Optimization

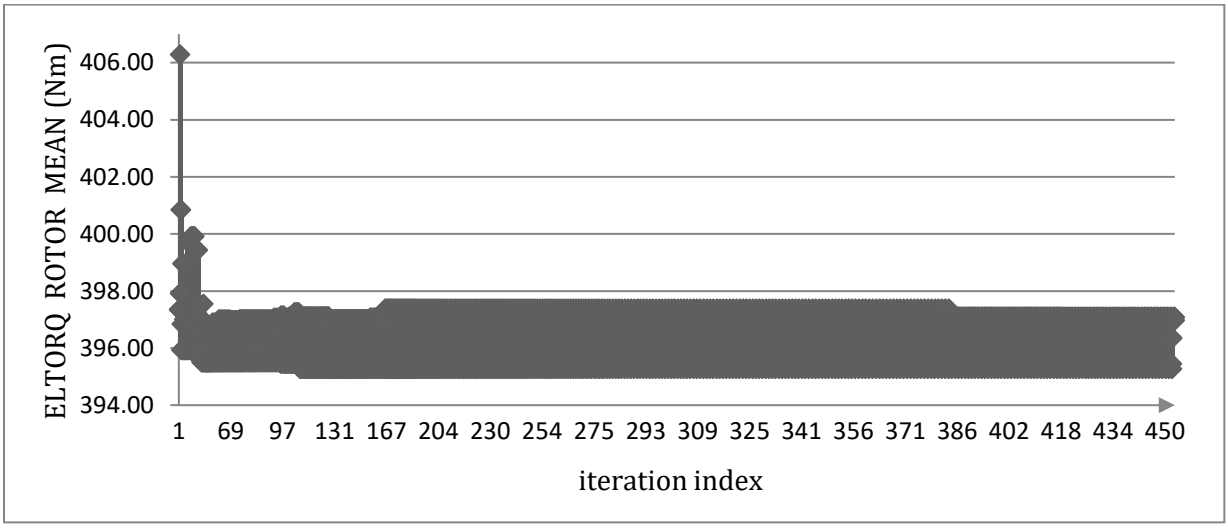

(a)

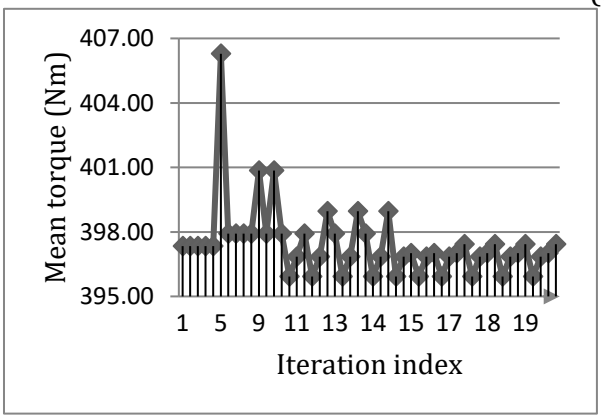

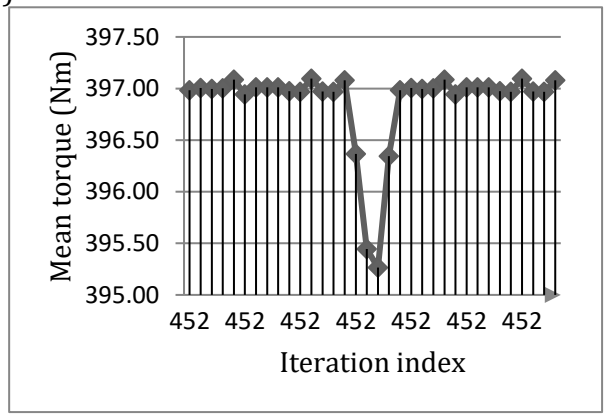

(b) (c)

Figure 30 : Iteration Plot : (a) Objective Function During Mean Torque Optimization, (b) Iterations 1–20 from the Original Iteration Plot of Mean Torque Optimization , (c) Iterations 450–452 from the Original Iteration Plot of Mean Torque Optimization

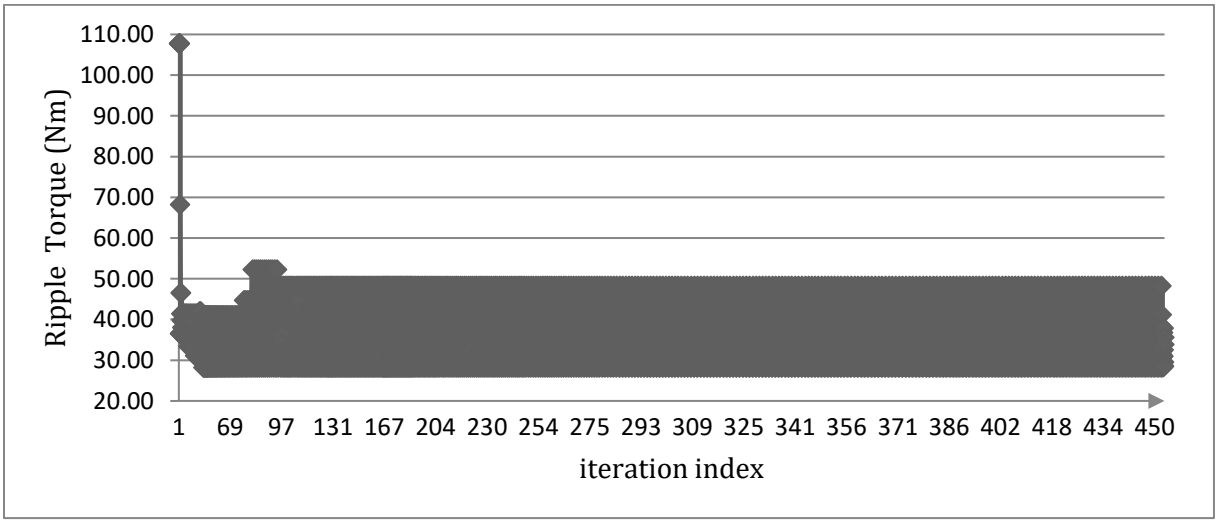

(a)

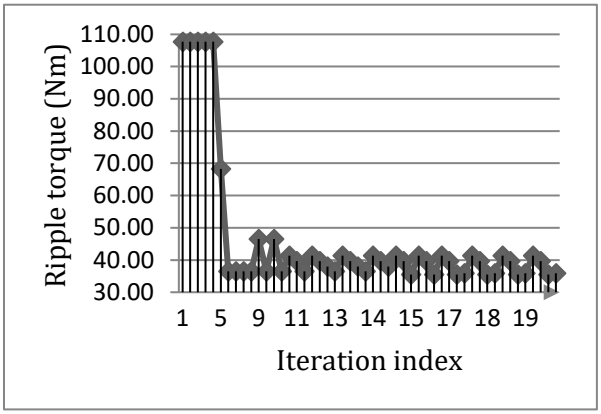

(b)

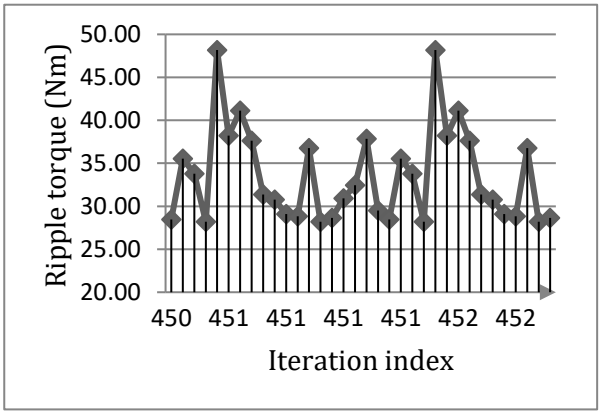

(c)

Figure 31 : Iteration Plot : (a) Objective Function During Ripple Torque Optimization, (b) Iterations 1–20 from the Original Iteration Plot of Ripple Torque Optimization , (c) Iterations 450–452 from the Original Iteration Plot of Ripple Torque Optimization

4.7.2 **post processing**

4.7.2.1 Optimal Points

4.7.2.1.1 Table Optimal Points

Table 21 : Optimal Points Selection After the Completion of Design Optimization

ID	BETAM	BRIDGE	IPMHQ	LM	LWEB	MAGWID	WEB	ELTORQ_ROTOR_MEAN	Magnet_area	Ripple_Torque	Goal
94	128.85571	1.0343094	10.213222	5.090378	2.762316	48.836496	10.521799	396.36665	248.59622	28.185462	Acceptable
228	126.00813	0.9012171	9.548581	4.914998	2.855696	48.828374	10.868559	395.44444	239.99134	48.178144	Acceptable
250	127.06737	0.9572827	9.955652	4.893857	2.874352	49.526170	10.978778	395.26446	242.37397	38.229543	Acceptable
252	126.30789	0.9036900	9.862235	4.971174	2.780767	48.755428	10.353393	396.34347	242.37171	41.127979	Acceptable
564	126.08225	0.9010369	9.563250	4.861835	2.774477	50.016817	10.693822	396.98433	243.17350	37.636592	Acceptable
796	126.51175	0.9000001	9.464355	4.836938	2.753430	50.452712	10.620901	397.00525	244.03664	31.368330	Feasible
953	126.76967	0.9056315	9.171812	4.848221	2.767501	50.443142	10.734763	396.99673	244.55948	30.769815	Acceptable
985	127.16879	0.9070422	9.282226	4.849492	2.795177	50.536611	10.705003	397.00338	245.07691	29.078996	Feasible
1044	127.26390	0.9150909	9.146143	4.854776	2.782418	50.604921	10.701473	397.08636	245.67556	28.836494	Feasible
1045	126.02229	0.9011994	9.528776	4.821102	2.859505	50.442864	10.971840	396.94169	243.19020	36.763538	Acceptable
1169	128.67736	0.9526358	9.838233	4.871637	2.923949	50.870521	10.895643	397.01266	247.82269	28.212866	Feasible
1316	128.53582	0.9036306	9.690462	4.950736	2.785051	49.689283	10.599133	397.01084	245.99850	28.660156	Feasible
1645	126.37295	0.9035389	9.535525	4.821442	2.736528	50.636077	10.571938	397.01013	244.13890	30.930621	Feasible
1671	126.20968	0.9013736	9.469382	4.824683	2.733253	50.499192	10.754879	396.97565	243.64258	32.456812	Acceptable
1753	126.03875	0.9003787	9.570117	4.849757	2.830013	50.139594	10.798385	396.96935	243.16486	37.838501	Acceptable
2023	126.94498	0.9017585	9.506492	4.846717	2.792901	50.491130	10.646719	397.09617	244.71621	29.522656	Feasible
2130	127.63521	0.9166000	9.231557	4.834059	2.757614	50.908849	10.773085	396.97178	246.09635	28.478488	Acceptable
2513	126.13970	0.9018222	9.799179	4.825592	2.751122	50.424467	10.900185	396.96842	243.32788	35.522904	Acceptable
2855	126.02727	0.9003021	9.614604	4.825571	2.696966	50.458723	10.744529	397.08053	243.49216	33.787146	Feasible

4.7.2.1.2 curve optimal points

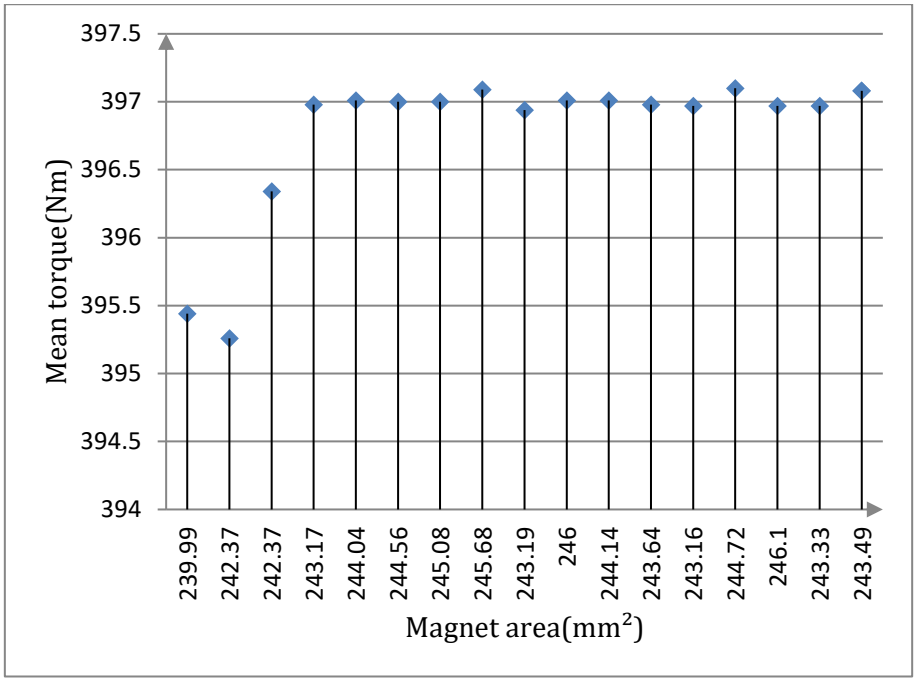

Figure 32 : Variation of mean torque as a Function of magnet area

4.7.3 **Design Geometry**

Evolution through the Optimization Process

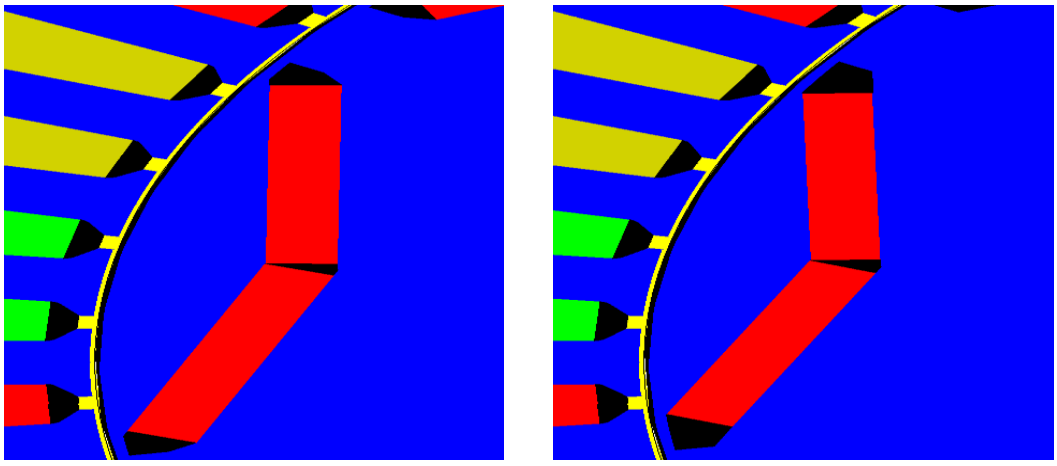

(a) (b)

Figure 33 : Design Geometry: (a)Before the optimization, (b)After the optimization

5 Simulation study of design optimization

5.1 case three

5.1.1 Graphical Comparison of Results Before and After Optimization

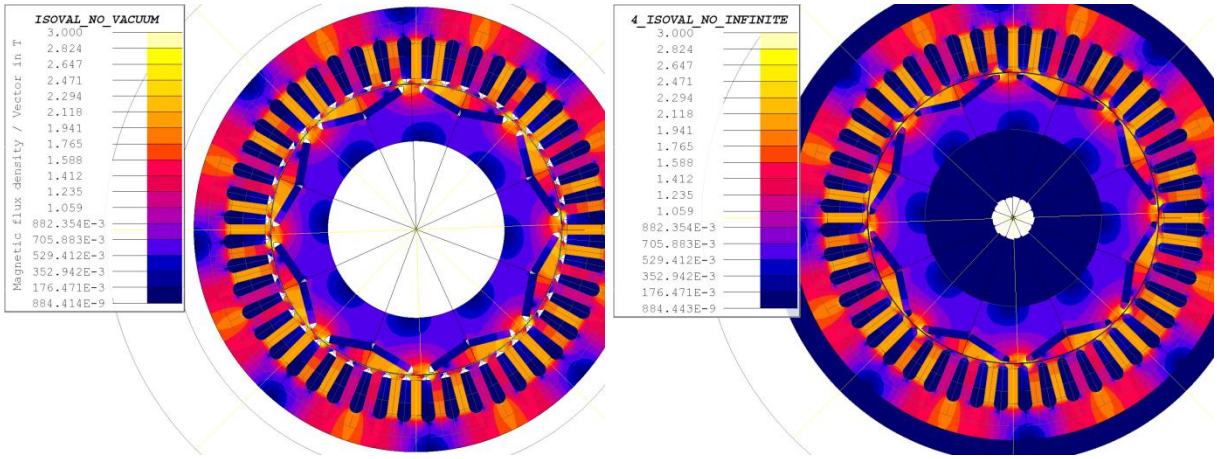

(a) (b)

Figure 34 : Graphical results of Isovalues of the magnetic flux density on surface regions : (a) Before, (b) After

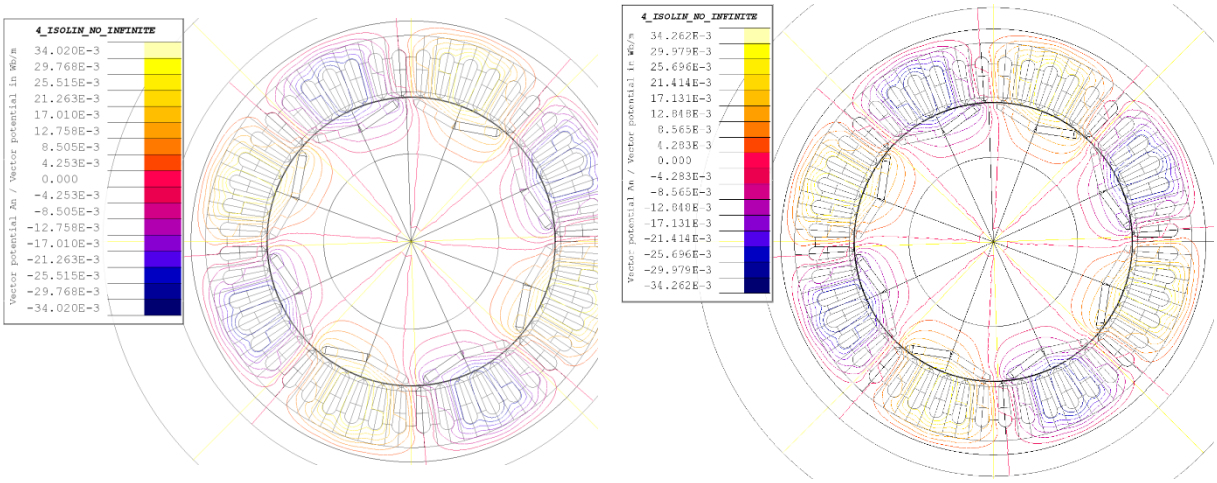

(a) (b)

Figure 35 : Graphical results of Isolines of the magnetic flux density on surface regions : (a) Before, (b) After

5.1.2 Curves Depicting the Behavior of the Optimized Design Solution

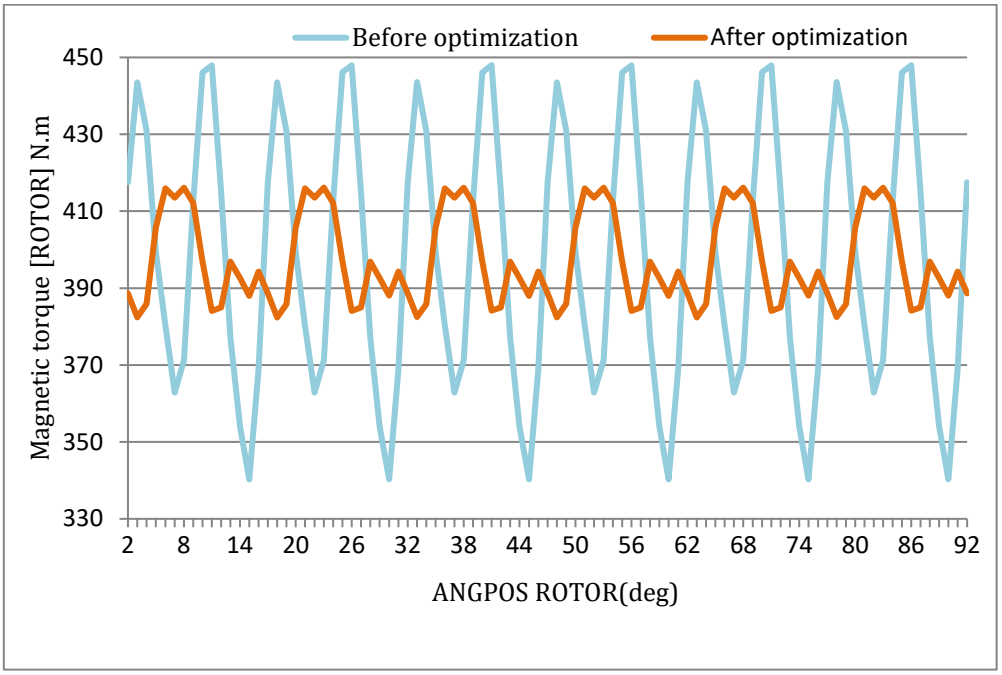

Figure 36 : Comparative Torque Curves Before and After Optimization

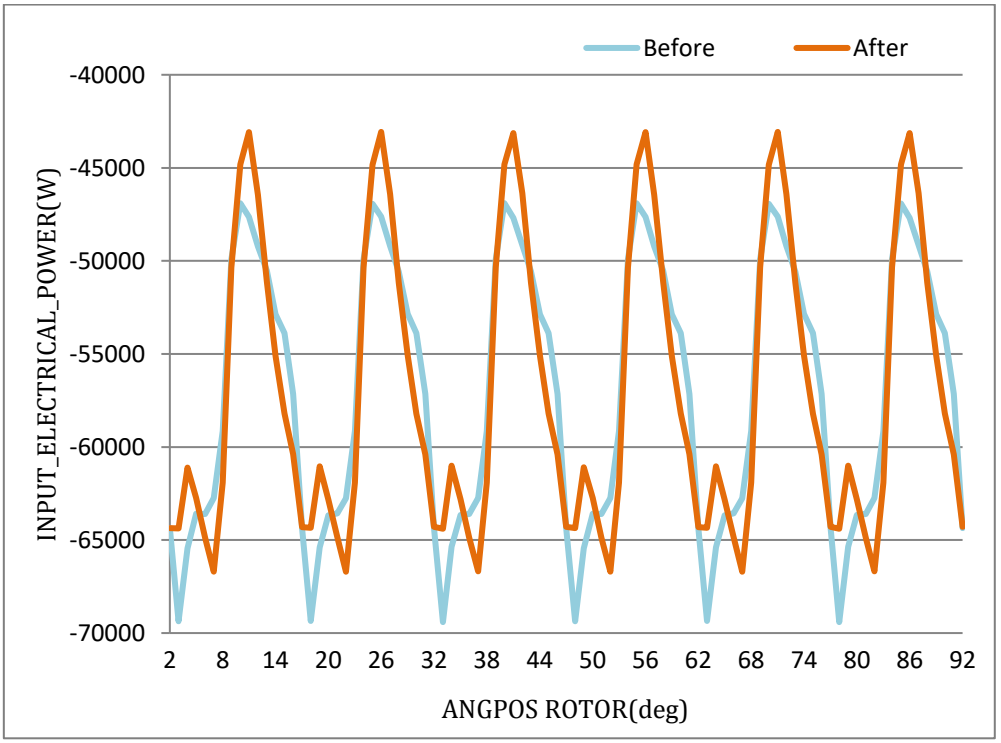

Figure 37 : Comparative power Curves Before and After Optimization

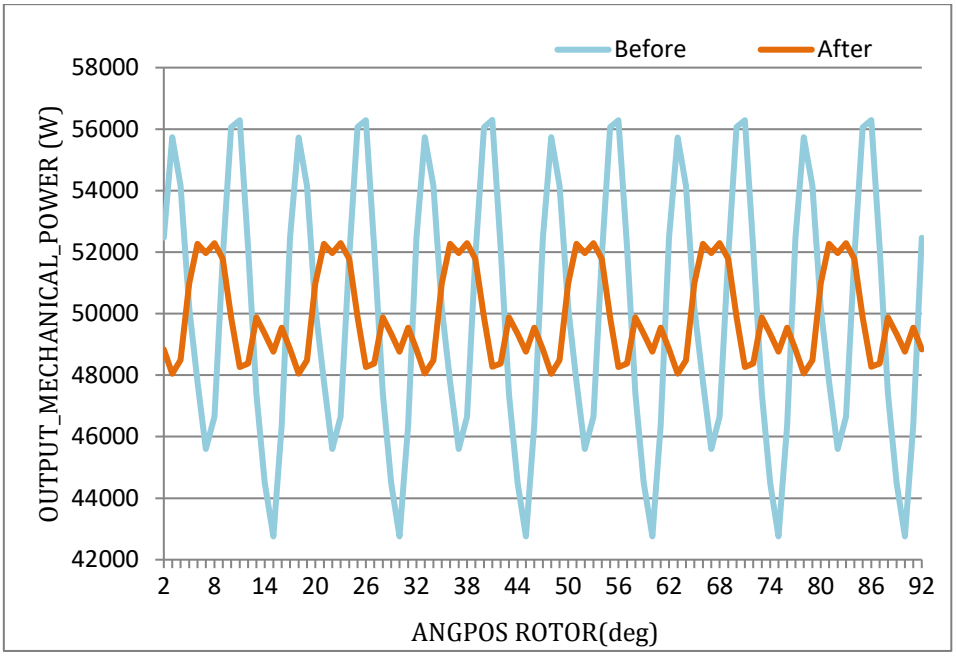

Figure 38 : Comparative power Curves Before and After Optimization

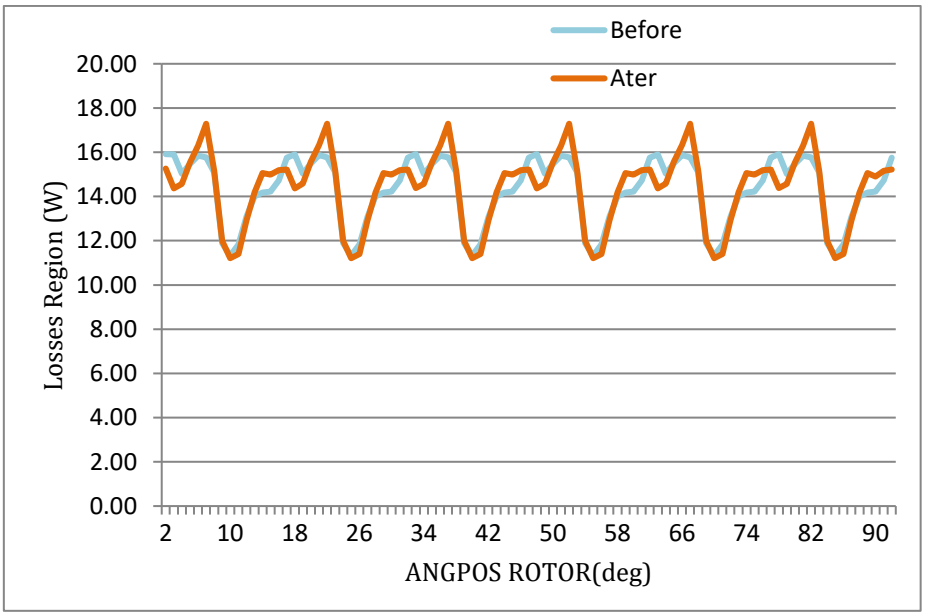

Figure 39 : Comparative loss region Curves Before and After Optimization

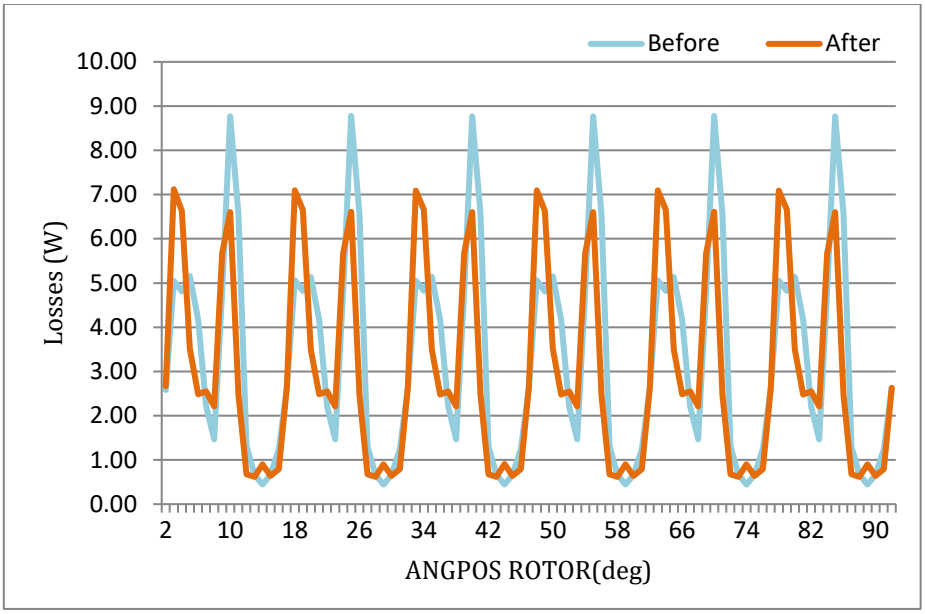

Figure 40 : Comparative magnet losses Curves Before and After Optimization

5.1.3 **Comparison between motor before and after optimization**

Table 22 : Optimal Design Parameter Values Obtained from Optimization of case three

Parameter	Before	After	Unit
Magnet Area	270	243.49 (9.81%↓)	mm^2
Torque_ Mean	397.34	397.08 (0.0665%↓)	Nm
Torque_ Max	447.97486	416.14 (7.106%↓)	Nm
Torque_ Min	340.25173	382.35 (12.372%↓)	Nm
Ripple torque	107.72313	33.787 (68.63%↓)	Nm
Input power	57092.1	57035.2 (0.0996%↓)	W
Output power	49996.9	49914.57 (0.164%↓)	W
Efficiency	87.57	87.52 (0.057%↓)	%
Iron losses	114.16	114.8 (%0.29↑)	W
Magnet losses	26.56	23.84 (10.24%↓)	W

5.2 case four

5.2.1 Graphical Comparison of Results Before and After Optimization

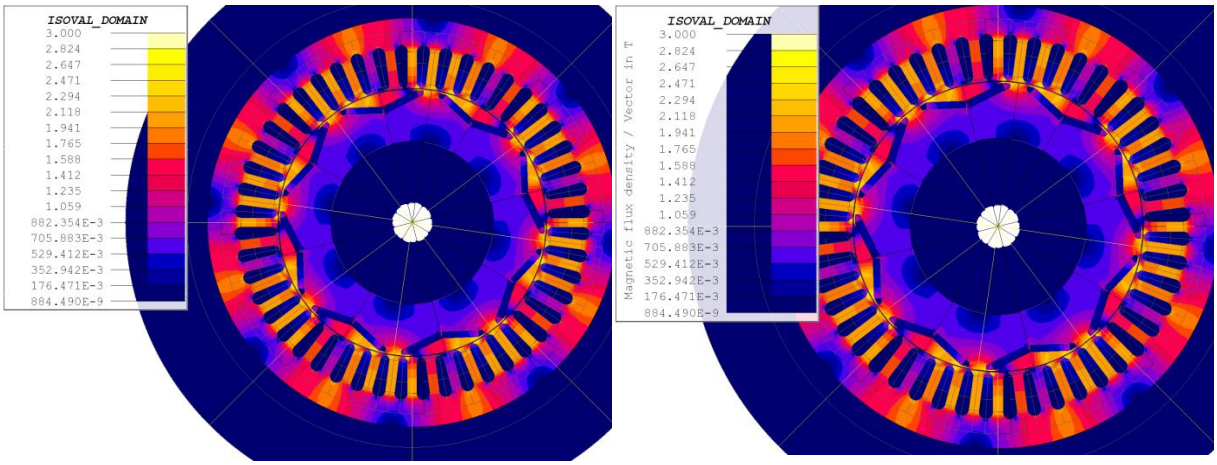

(a) (b)

Figure 41 : Graphical results of Isovalues of the magnetic flux density on surface regions : (a) Before, (b) After

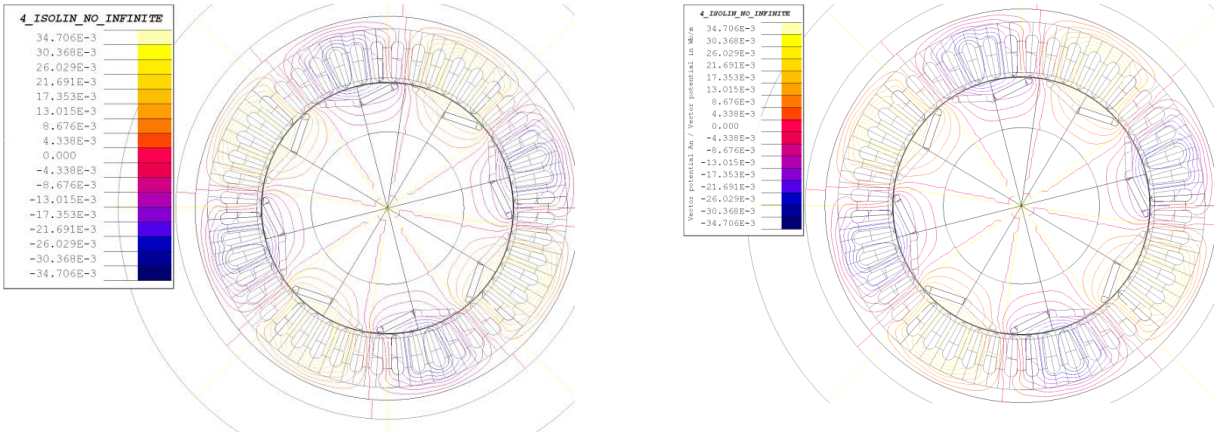

(a) (b)

Figure 42 : Graphical results of Isolines of the magnetic flux density on surface regions : (a) Before, (b) After

5.2.2 Curves Depicting the Behavior of the Optimized Design Solution

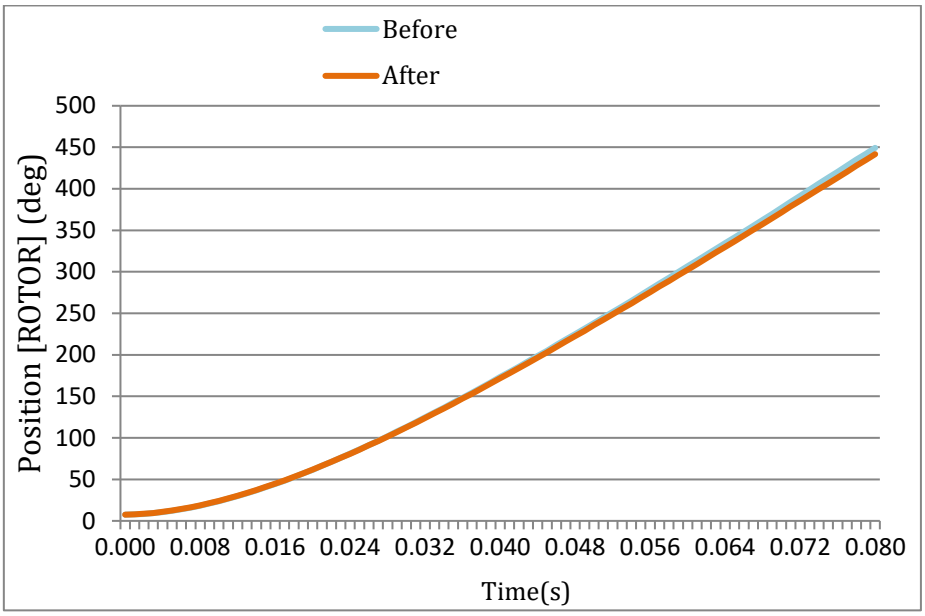

Figure 43 : Comparative Position Curves Before and After Optimization

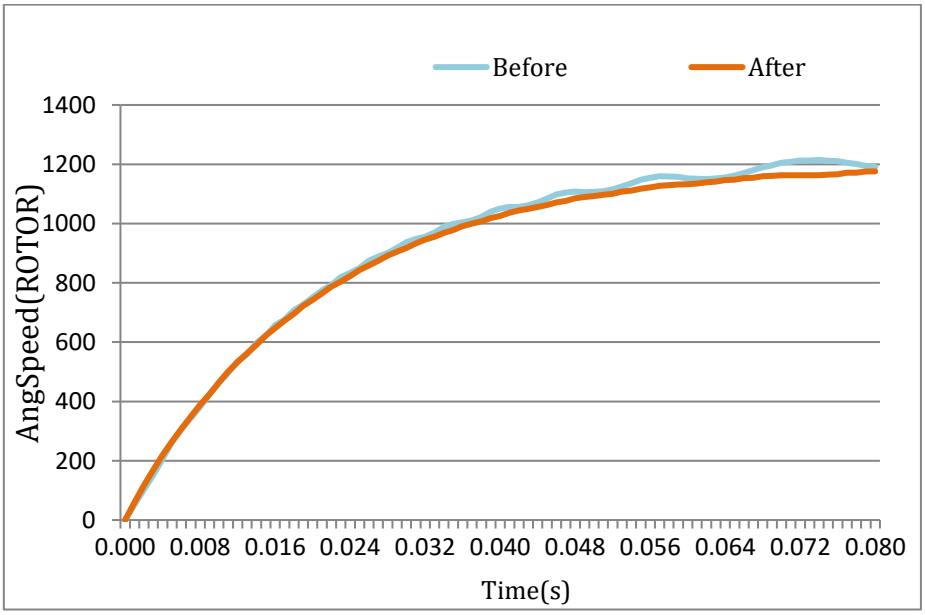

Figure 44 : Comparative AngSpeed Curves Before and After Optimization

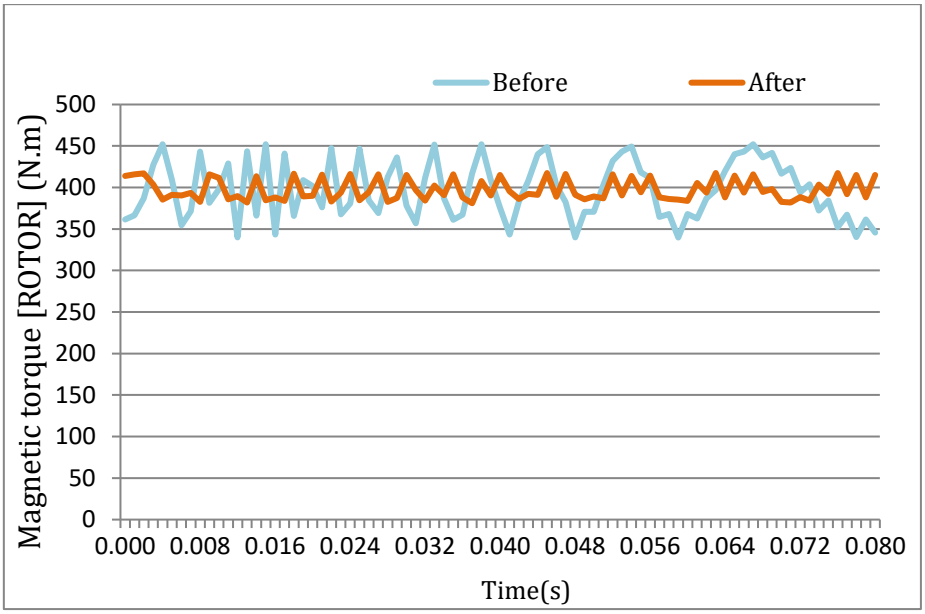

Figure 45 : Comparative Magnetic torque Curves Before and After Optimization

5.2.1 **Comparison between motor before and after optimization**

Table 23 : Optimal Design Parameter Values Obtained from Optimization of case four

Parameter	Before	After	Unit
Magnet Area	270	243.49 (9.81%↓)	mm^2
Torque_ Mean	397.62	397.36 (0.07%↓)	Nm
Torque_ Max	452.11	417.48 (7.66%↓)	Nm
Torque_ Min	339.76	381.08 (12.16%↑)	Nm
Ripple torque	112.35	36.4 (67.59%↓)	Nm
Current_ Mean(I1)	15.09	14.74 (2.32%↓)	A
Current_ Mean(I2)	-5.07	2.21 (56.40%↓)	A
Current_ Mean(I3)	-10.02	12.53 (25.03%↑)	A
Speed_Mean	913.08	897.29 (1.73%↓)	rpm

6 Result Analysis

In Case 3, the optimization led to a reduction in the magnet area from 270 mm^2 to 243.49 mm^2, which helps reduce material costs without significantly affecting performance. The mean torque slightly decreased from 397.34 Nm to 397.08 Nm, showing that torque performance was preserved. However, a notable reduction in maximum torque was achieved (from 447.97 Nm to 416.14 Nm), while the minimum torque increased significantly (from 340.25 Nm to 382.35 Nm). This improvement results in a much lower torque ripple, which dropped from 107.72 Nm to 33.78 Nm – a key benefit that enhances the smoothness of operation and mechanical reliability.

In terms of energy performance, input power slightly decreased from 57092.1 W to 57035.2 W, and output power from 49996.9 W to 49914.57 W, keeping efficiency nearly unchanged (87.57% to 87.52%). Iron losses slightly increased, possibly due to modifications in magnetic flux distribution, while magnet losses decreased from 26.56 W to 23.84 W, thanks to the reduced magnet volume.

For Case 4, similar trends are observed. The magnet area was also reduced by 9.81%. The mean torque remained nearly the same (397.62 Nm to 397.36 Nm), ensuring that the main performance indicator was maintained. However, maximum torque dropped by 7.66%, while minimum torque increased by 12.16%. As a result, the torque ripple dropped dramatically by 67.59% (from 112.35 Nm to 36.4 Nm), confirming that the optimization succeeded in producing smoother torque.

In addition, phase current values showed significant changes: I1 decreased slightly, I2 decreased by over 56%, and I3 increased by 25%. These variations reflect a more balanced phase current distribution, which contributes to reducing electromagnetic noise and losses. The mean of rotational speed slightly decreased (1.73%), which remains acceptable in most practical applications.

Overall, the optimization of both cases achieved a remarkable reduction in torque ripple, improved the balance of torque values, reduced magnet material, and preserved efficiency, making the proposed motor designs more effective for high-performance and cost-sensitive applications.

7 Conclusion

The optimization studies carried out in this work for both Case 3 and Case 4 have demonstrated the effectiveness of the proposed design approach. By using numerical simulations based on finite element analysis (FEA), the PMSM with interior magnets was carefully refined to improve torque quality and reduce material usage without compromising overall efficiency.

In both cases, a significant reduction in torque ripple was achieved – over 60% – while keeping the mean torque nearly constant. These results are highly favorable for applications requiring smooth and stable motor operation, such as electric vehicles and robotics. Additionally, the magnet area was reduced, which contributes directly to lowering the cost and weight of the machine.

The changes observed in current distribution and loss components confirm that the optimization successfully balanced the electromagnetic performance. Despite a slight reduction in speed and a minimal variation in efficiency, the overall behavior of the motor improved in terms of mechanical and dynamic performance.

In conclusion, the optimized design presents a more cost-effective, stable, and efficient solution for interior permanent magnet synchronous motors (IPMSMs), offering a solid foundation for further developments and real-world applications.

General conclusion

This work provided a comprehensive analysis of the Interior Permanent Magnet Synchronous Motor (IPMSM), combining theoretical modeling with numerical simulations based on the Finite Element Method to gain a deep understanding of how design variables influence key performance metrics such as torque, efficiency, and losses.

The obtained results clearly demonstrated that optimizing the shape and placement of the embedded magnets in the rotor can significantly reduce torque ripple, increase minimum torque, and decrease the amount of magnetic material required, all while maintaining or even improving efficiency. This balance between performance and material savings is essential in the context of high-efficiency electric drive systems. Furthermore, the application of multi-objective optimization through HyperStudy proved highly effective in finding a trade-off between various design goals, offering a more refined and reliable approach than traditional trial-and-error methods.

Looking ahead, the ongoing evolution of digital technologies and artificial intelligence (AI) presents exciting opportunities for further enhancement. AI-powered methods, such as machine learning and reinforcement learning, have the potential to revolutionize the optimization process by analyzing massive datasets, predicting motor behavior under varying conditions, and even generating innovative design solutions autonomously.

When integrated with advanced platforms like HyperStudy and Flux, AI-based optimization can transform the entire design workflow into a smart, adaptive, and data-driven process, significantly reducing development time and cost while unlocking new levels of motor performance. These future perspectives suggest a promising path toward even more efficient, compact, and intelligent electric motors, playing a crucial role in the next generation of sustainable energy and transportation systems.

References

[1] W. Pan, H. Zhu, and H. Li, "Design and optimization of bearingless permanent magnetic synchronous motors," *IEEE Transactions on Applied Superconductivity,* vol. 26, no. 4, pp. 1-1, 2016.

[2] A. Dalcalı, "Optimal design of high performance interior PM motor for electric vehicle," *The International Journal of Energy and Engineering Sciences,* vol. 3, no. 2, pp. 46-54, 2018.

[3] V. Sarac, "OPTIMIZATION AND ANALYSIS OF AN INTERIOR PERMANENT MAGNET SYNCHRONOUS MOTOR," *Journal of Energy Technology,* vol. 16, no. 3, pp. 35-44, 2023.

[4] T. Gundogdu and G. Komurgoz, "The Impact of the selection of permanent magnets on the design of permanent magnet machines–a case study: permanent magnet synchronous machine design with high efficiency," *Przeglqd Elektrotechniczny R89,* pp. 103-108, 2013.

[5] L. KNEBL, "Design and optimization of high-torque ferrite assisted synchronous reluctance motor," *Brno: University of Technology in Brno, Faculty of Electrical Engineering and commu nication,* 2021.

[6] M. Ibragimov, D. Akbarov, M. Fayziyev, R. Beytullaeva, K. Nimatov, and K. S. Safarov, "Analysis of the methods of diagnosing asynchronous motors according to vibration indicators," in *IOP Conference Series: Earth and Environmental Science*, 2023, vol. 1142, no. 1, p. 012031: IOP Publishing.

[7] A. Daanoune, "Contribution à l'etude et à l'optimisation d'une machine synchrone à double excitation pour véhicules hybrides," Université de Grenoble, 2012.

[8] D. Ocean, "Direct Torque Control of a Permanent Magnet synchronous Motor," *Master's Degree Project, KTH Royal Institute of Technology in Stockholm, Stockolm,* 2005.

[9] A. El-Shahat and M. Ruba, *Applied electromechanical devices and machines for electric mobility solutions*. BoD–Books on Demand, 2020.

[10] J. M. Coey, "Permanent magnet applications," *Journal of Magnetism and Magnetic Materials,* vol. 248, no. 3, pp. 441-456, 2002.

[11] T. Heikkilä, "Permanent magnet synchronous motor for industrial inverter applications-analysis and design," 2002.

[12] B. Boukais, "Contribution à la modélisation des systèmes couples machines convertisseurs: Application aux machines à aimants permanents (BDCM-PMSM)," Université Mouloud Mammeri, 2012.

[13] E. Bommé, "Modélisation et optimisation des machines électriques discoïdes à double entrefer," Institut National Polytechnique de Grenoble-INPG, 2009.

[14] I. Petrov and J. Pyrhonen, "Performance of low-cost permanent magnet material in PM synchronous machines," *IEEE transactions on Industrial Electronics,* vol. 60, no. 6, pp. 2131-2138, 2012.

[15] X. Liu, Q. Lin, and W. Fu, "Optimal design of permanent magnet arrangement in synchronous motors," *Energies,* vol. 10, no. 11, p. 1700, 2017.

[16] N. Bracikowski, "Modélisation multi-physique par modèles à constantes localisées; application à une machine synchrone à aimants permanents en vue de son dimensionnement," Ecole Centrale de Lille, 2012.

[17] A. Balashanmugham and M. Maheswaran, "Permanent-magnet synchronous machine drives," in *Applied Electromechanical Devices and Machines for Electric Mobility Solutions*: IntechOpen, 2019.

[18] P. Salminen, "Fractional slot permanent magnet synchronous motors for low speed applications," 2004.

[19] S. Morimoto, "Trend of permanent magnet synchronous machines," *IEEJ Transactions on Electrical and Electronic Engineering,* vol. 2, no. 2, pp. 101-108, 2007.

[20] J. F. Gieras, *Permanent magnet motor technology: design and applications*. CRC press, 2009.

[21] A. Waheed and J. Ro, "Analytical modeling for optimal rotor shape to design highly efficient line-start permanent magnet synchronous motor," *IEEE access,* vol. 8, pp. 145672-145686, 2020.

[22] Y. Guo, J. Si, C. Gao, H. Feng, and C. Gan, "Improved fuzzy-based Taguchi method for multi-objective optimization of direct-drive permanent magnet synchronous motors," *IEEE transactions on magnetics,* vol. 55, no. 6, pp. 1-4, 2019.

[23] A. Ayppachan, "Study of three phase symmetrical short circuit for test analysis and demagnetization impact in IPMSM: Analysis of pre-fault short circuit conditions, demagnetization effects and impact of a second short circuit in IPMSM," ed, 2024.

[24] M. BECHEIKH and S. HASSAIN, "Co-Simulation of permanent magnet synchronous motor with demagnetized fault fed by PWM inverter," *Przeglad Elektrotechniczny,* vol. 2024, no. 4, 2024.

[25] M. Chowdhury, M. Islam, and A. Gebregergis, "Parameter characterization and performance prediction of permanent magnet synchronous motor for high performance applications," in *2018 IEEE Transportation Electrification Conference and Expo (ITEC)*, 2018, pp. 1135-1140: IEEE.

[26] M. Jeannerot, M. Ouisse, V. Lanfranchi, J. B. Dupont, and E. Sadoulet-Reboul, "Two-level global sensitivity analysis of the excitation contributions leading to acoustic noise in an electric motor for the purpose of robust optimisation," *IET Electric Power Applications,* vol. 15, no. 12, pp. 1666-1677, 2021.

[27] M. Huikuri, "Modelling and Disturbance Compensation of a Permanent Magnet Linear Motor with a Discontinuous Track," 2019.

[28] I. Shuaibu, E. H. T. Wei, R. Kannan, and Y. A. Samaila, "The Utilization of Printed Circuit Boards (PCBs) in Axial Flux Machines: A Systematic Review," *Engineering Proceedings,* vol. 87, no. 1, p. 13, 2025.

[29] X. Wei, Z. Ma, X. Zhu, and Y. Zheng, "An Analysis of the Safety of Low-Speed Electric Vehicles in the Event of a Frontal Collision," SAE Technical Paper0148-7191, 2021.

[30] M. Z. M. Jaffar, *Modeling and analysis of saturated inductances and torque ripple components in interior permanent magnet motors*. North Carolina State University, 2019.

[31] H. Khawaja, "Windtech Technology-Measuring Cold Exposure via Conjugate Heat Transfer," 2020.

[32] M. H. Chowdhury, *Rare-Earth Free Electric Machine for High Performance Applications*. North Carolina State University, 2021.

[33] A.-I. Constantin, C. Dumitru, E. Tudor, I. Vasile, and M. Arsene, "Studies related to the optimization of an interior permanent magnet synchronous machine designed for the electric vehicles," in *2021 International Conference on Applied and Theoretical Electricity (ICATE)*, 2021, pp. 1-5: IEEE.

[34] V. Ghorbanian, M. H. Mohammadi, I. Ibrahim, D. A. Lowther, and J. Hendershot, "An HPC-based data-driven process for design exploration and optimization of motor drives," in *2019 IEEE International Electric Machines & Drives Conference (IEMDC)*, 2019, pp. 597-602: IEEE.

[35] S. Schiettecatte, "Multi-Objective Design Optimization of Energy-Saving Electrical Machine Windings Enabled by Additive Manufacturing."

[36] L. Mariolo, A. Rubino, D. Spelta, and L. Frosini, "Modeling of hybrid stepper motor finalized to the optimization of the holding torque," in *2021 IEEE Workshop on Electrical Machines Design, Control and Diagnosis (WEMDCD)*, 2021, pp. 107-112: IEEE.

[37] N. Mazgaonkar, M. Chowdhury, and L. F. Fernandes, "Design of electric motor using coupled electromagnetic and structural analysis and optimization," SAE Technical Paper0148-7191, 2019.

[38] R. Notari, G. Devito, S. Nuzzo, D. Barater, M. Degano, and C. Gerada, "Analytical-FE Study of Rotor-Dependent Hairpin Conductor Sizing in High-Performance IPMSMs," in *2025 IEEE Workshop on Electrical Machines Design, Control and Diagnosis (WEMDCD)*, 2025, pp. 1-6: IEEE.

[39] S. Paul and J. Chang, "Fast model-based design of high performance permanent magnet machine for next generation electric propulsion for urban aerial vehicle application," *CES Transactions on Electrical Machines and Systems,* vol. 5, no. 2, pp. 143-151, 2021.

[40] S. Balaji, "Modelling and Simulation of Interior Permanent Magnet Synchronous Machine and, Design Optimization Towards Transmission," ed, 2022.

[41] M. E. Abdollahi, "Design of a Switched Reluctance Motor for a Light Sport Aircraft Application," 2022.

[42] D. Liu, "Development of a hybrid algorithm for efficiently solving mixed integer-continuous optimization problems," *Applied and Computational Mathematics,* vol. 5, no. 3, pp. 107-113, 2016.

[43] M. S. Islam, M. A. Kabir, R. Mikail, and I. Husain, "Interactive ripple harmonic minimization of fractional slot permanent magnet machines using space-shifted wye-delta winding," in *2019 IEEE International Electric Machines & Drives Conference (IEMDC)*, 2019, pp. 288-294: IEEE.

[44] M. Chowdhury, M. S. Islam, and M. Islam, "Design optimization of interior permanent magnet synchronous machines utilizing global response surface method for variable speed drives," in *2019 IEEE International Electric Machines & Drives Conference (IEMDC)*, 2019, pp. 609-614: IEEE.

[45] W. Guendouz, A. Tounzi, and T. Rekioua, "Design of quasi-halbach permanent-magnet vernier machine for direct-drive urban vehicle application," *Machines,* vol. 11, no. 2, p. 136, 2023.

[46] M. Caruso, A. Di Tommaso, R. Miceli, C. Nevoloso, C. Spataro, and F. Viola, "Characterization of interior permanent magnet synchronous motors for loss model algorithm identification," in *21st IMEKO TC-4 International Symposium on Understanding the World through Electrical and Electronic Measurement, and 19th International Workshop on ADC Modelling and Testing*, 2016, pp. 37-42.